A SURVEY FOR CIRCUMSTELLAR DISKS AROUND YOUNG SUBSTELLAR OBJECTS

Joan Najita

National Optical Astronomy Observatory, 950 North Cherry Avenue, Tucson, AZ 85719 ${\rm ALAN~T.~TOKUNAGA}$

Institute for Astronomy, University of Hawaiʻi, 2680 Woodlawn Drive, Honolulu, HI 96822 Astrophysical Journal, $in\ press$

ABSTRACT

We have completed the first systematic survey for disks around spectroscopically identified young brown dwarfs and very low mass stars. For a sample of 38 very cool objects in IC 348 and Taurus, we have obtained L'-band (3.8 μ m) imaging with sufficient sensitivity to detect objects with and without disks. The sample should be free of selection biases for our purposes. Our targets span spectral types from M6 to M9.5, corresponding to masses of \sim 15 to 100 M_{Jup} and ages of \lesssim 5 Myr based on current models. None appear to be binaries at 0".4 resolution (55–120 AU). Using the objects' measured spectral types and extinctions, we find that most of our sample $(77\% \pm 15\%)$ possess intrinsic IR excesses, indicative of circum(sub)stellar disks. Because the excesses are modest, conventional analyses using only IR colors would have missed most of the sources with excesses. Such analyses inevitably underestimate the disk fraction and will be less reliable for young brown dwarfs than for T Tauri stars. The observed IR excesses are correlated with $H\alpha$ emission, consistent with a common accretion disk origin. In the same star-forming regions, we find that disks around brown dwarfs and T Tauri stars are contemporaneous; assuming coevality, this demonstrates that the inner regions of substellar disks are at least as long-lived as stellar disks and evolve slowly for the first ~ 3 Myr. The disk frequency appears to be independent of mass. However, some objects in our sample, including the very coolest (lowest mass) ones, lack IR excesses and may be diskless. The observed excesses can be explained by disk reprocessing of starlight alone; the implied accretion rates are at least an order of magnitude below typical values for classical T Tauri stars. The observed distribution of IR excesses suggests inner disk holes with radii of $\gtrsim 2R_{\star}$, consistent with the idea that such holes arise from disk-magnetosphere interactions. Altogether, the frequency and properties of young circumstellar disks appear to be similar from the stellar regime down to the substellar and planetary-mass regime. This provides prima facie evidence of a common origin for most stars and brown dwarfs.

Subject headings: stars: low-mass, brown dwarfs — infrared: stars

1. INTRODUCTION

Brown dwarfs are now being found in abundance. In the solar neighborhood, the advent of very wide-field sky surveys have led to the discovery of hundreds of nearby ultracool dwarfs, many of which are likely to be substellar (e.g. Kirkpatrick et al. 1999; Delfosse et al. 1999; Burgasser et al. 2002; Hawley et al. 2002). Discoveries of more distant substellar objects are increasing as deep, blank sky surveys become more powerful (e.g. Cuby et al. 1999; Liu et al. 2002). Likewise, surveys of nearby open clusters, in particular the Pleiades, have been very successful at identifying brown dwarfs (e.g. Bouvier et al. 1998; Stauffer et al. 1998; Moraux et al. 2001). Searches of young ($\leq 10 \text{ Myr}$) star-forming regions have also been quite rewarding. Substellar objects are hotter and more luminous in their youth, and hence it is feasible to probe to very low masses in star-forming regions (e.g. Luhman et al. 2000; Najita et al. 2000; Zapatero Osorio et al. 2000; Lucas et al. 2001; Liu 2001). Though mass determinations for such young objects are necessarily dependent on theoretical models, the coolest objects seem to be $\lesssim 15 M_{Jup}$, comparable in mass to planets around old solar-type stars found from radial velocity studies (e.g. Marcy & Butler 1998).

While the number of known brown dwarfs is growing rapidly, the origin of these objects is an unanswered question. The initial mass function (IMF) measured in young clusters seems to be continuous from the stellar to substellar regime (e.g. Hillenbrand & Carpenter 2000; Najita et al. 2000), suggesting brown dwarfs form in the same manner as stars. However, the overlap in mass between young "planetary-mass" brown dwarfs ($\lesssim 15 M_{Jup}$) and planets discovered by radial velocity surveys is intriguing, maybe suggestive of a common genesis in disks around young stars. However, it is unlikely such brown dwarfs could form like giant planets are believed to, namely core accretion followed by runaway growth (Pollack et al. 1996). Perhaps gravitational disk instabilities (Boss 1998; Pickett et al. 2000) or disk-disk collisions (Lin et al. 1998; Watkins et al. 1998a,b) are involved, followed by ejection into the field. Indeed, a few solar-type stars are known to have massive substellar companions (Els et al. 2001; Marcy et al. 2001; Liu et al. 2001; Potter et al. 2002; Udry

¹ Beatrice Watson Parrent Fellow.

et al. 2002), which might point to concurrent formation of brown dwarfs and planets. An alternative formation scenario involving ejection has been proposed by Reipurth & Clarke (2001). They suggest that brown dwarfs form as stellar embryos in small newborn multiple systems, but their growth is prematurely truncated by ejection due to dynamical interactions at very young ages ($\sim 10^4$ yr). A recent computer simulation of cloud fragmentation by Bate et al. (2002) portrays an amalgam of these scenarios: most brown dwarfs form via gravitational instabilities in circumstellar disks and then are ejected before they can accrete to stellar masses.

The abundance of isolated brown dwarfs in star-forming regions and open clusters stands in stark contrast to the dearth of 20– $70~M_{Jup}$ objects found as close radial velocity companions to mature, solar-type stars, a.k.a. the "brown dwarf desert" (Campbell et al. 1988; Marcy & Benitz 1989; Walker et al. 1995; Halbwachs et al. 2000; Zucker & Mazeh 2001; Pourbaix & Arenou 2001). But the implication of this phenomenon is unclear. It might suggest that isolated brown dwarfs and massive planetary companions arise from independent formation pathways. Alternatively, the difference might stem from evolutionary effects which preferentially deplete brown dwarf companions, such as inward migration into the central star (Armitage & Bonnell 2002) or outward ejection.

One potential insight into the formation mechanism(s) for brown dwarfs is whether young substellar objects possess circumstellar disks. There is abundant observational evidence for accretion disks around young solar-type stars. Moreover, disks are a key element in current theoretical understanding of star and planet creation: the formation of a disk is believed to be an inevitable step, since the infalling natal material has angular momentum. Thus, the presence of disks around young brown dwarfs is naturally accommodated in "star-like" formation scenarios. On the other hand, scenarios involving collision and/or ejection are likely to be hostile to circumstellar disks. Hence, determining the frequency and physical properties of disks around young brown dwarfs, as well as their relation to disks around young stars, is an important observational goal.

Evidence for circumstellar disks around individual young (\(\sigma\) few Myr) brown dwarfs has recently been found. Strong H α emission, likely due to ongoing accretion, has been seen from sources in Taurus (Briceño et al. 1998; Martin et al. 2001), IC 348 (Luhman 1999), ρ Oph (Luhman et al. 1997), and σ Ori (Barrado y Navascués et al. 2001; Zapatero Osorio et al. 2002a,b). Direct kinematic evidence for accretion from asymmetric $H\alpha$ emission line profiles has been found for one object in Taurus at the substellar mass limit (Muzerolle et al. 2000). Infrared (IR) excesses have been detected from JHK $(1.1-2.4 \mu m)$ data for a few spectroscopically identified young brown dwarfs in ρ Oph (Wilking et al. 1999; Cushing et al. 2000), IC 348 (Luhman 1999), and the Trapezium cluster (Hillenbrand et al. 1998; Lucas et al. 2001). A recent JHK survey by Muench et al. (2001) finds a majority of photometrically selected brown dwarf candidates in Trapezium have excesses.

IR excesses are one of the classic signatures for disks around T Tauri stars. Such excesses are correlated with

UV/optical excess emission, as expected for an accretion disk origin (Hartigan et al. 1990; Valenti et al. 1993; Edwards 1995; Kenyon & Hartmann 1995). In particular, there is a one-to-one correspondence between IR color excesses and optical veiling indicative of accretion onto the central source (Hartigan et al. 1995). There is other plentiful evidence for disks around T Tauri stars, including far-IR photometry, millimeter wavelength studies, and highresolution optical/IR imaging — for nearly all objects, the different disk indicators agree, which supports the accuracy of using a single indicator, in this case IR excess. On physical grounds, disks are the best explanation for both the IR excesses and the relatively low extinctions to the central sources (e.g. Adams & Shu 1986; Myers et al. 1987). This body of evidence naturally explains the IR excesses detected from young brown dwarfs as originating from circumstellar disks.

Mid-IR (7–14 μ m) detections are available for young brown dwarfs in ρ Oph (Comerón et al. 1998; Bontemps et al. 2001; Testi et al. 2002; Natta et al. 2002) and Chamaeleon (Comerón et al. 2000; Natta & Testi 2001; Apai et al. 2002), which further support the disk hypothesis. The mid-IR fluxes are $\gtrsim 10\times$ greater than expected from the photosphere, and the resulting spectral energy distributions (SEDs) are much broader than can be explained by a non-disk origin.

However, it is difficult to determine the frequency of disks around brown dwarfs from studies to date due to a combination of small number statistics, sample selection inhomogeneity, and, most importantly, choice of wavelength. A priori, brown dwarf disks are expected to be harder to detect than disks around stars because of lower contrast. Substellar objects are less luminous and have shallower gravitational potentials; hence, the inner regions of their disks are likely to be cooler and thus could have negligible excesses in the JHK bands, which have been used by most previous studies. Disks are more luminous at longer wavelengths, and they can be readily identified at mid-IR wavelengths. But because such observations can only detect young brown dwarfs with large excesses, a complete census of the disk frequency is not yet possible in the mid-IR.

L'-band (3.8 μ m) observations are an excellent means to address this question. Disks can be readily identified from ground-based telescopes by excess L'-band emission, which arises from warm circumstellar material within a few stellar radii ($\lesssim 0.1~{\rm AU}$). In addition, existing infrared cameras can detect young brown dwarf photospheres, and hence the absence of a disk can be discerned. Such observations have been used to measure the disk frequency for low-mass stars in young clusters (e.g., Haisch et al. 2000). These studies find a higher disk frequency than JHK or $H\alpha$ studies, as expected from the greater sensitivity of thermal IR observations to less luminous disks.

In this paper, we present results from a large L'-band survey for circumstellar disks around young brown dwarfs and very low mass (VLM) stars in the IC 348 and Taurus star forming regions. The incidence and properties of disks around young substellar objects may shed light on the origin of these intriguing objects. Our study targets young sources which have been *spectroscopically classified* to be very cool, with spectral types of M6 and later. By focus-

ing on targets with spectral types, we are more sensitive to small IR excesses since we can determine the intrinsic photospheric colors. Our selection criterion also ensures that we are targeting very low mass members, lying near or below the stellar/substellar mass boundary. Since our observations are sensitive enough to detect bare photospheres, this is the first unbiased survey for disks around such objects.

We describe our sample and our observations in \S 2. We discuss the frequency of IR excesses and correlations with other properties in \S 3. Simple models are used to study the disk characteristics in \S 4. We examine the possible systematic effects in \S 5. We then discuss the implications of our findings for brown dwarf disk searches, the properties of such disks, and brown dwarf formation scenarios in \S 6. Finally, we summarize our results in \S 7. For readers primarily interested in the results, we suggest focusing on \S 6 and \S 7.

2. Observations

2.1. Sample Selection and Properties

For objects in young star-forming regions, the substellar boundary is believed be around spectral type M6, based on comparison with theoretical models (Luhman et al. 1998a) and the application of the lithium test in young clusters (Basri 1998). Most young brown dwarf candidates do not have lithium measurements, which would guarantee their status as cluster members. However, their positions in color-magnitude diagrams indicate they are very likely cluster members and the very late spectral types are consistent with substellar status.

Our sample of 38 objects includes nearly all published objects with spectral types of M6 or later in the IC 348 and Taurus star-forming regions. We adopt a distance of 140 pc to Taurus (Elias 1978; Kenyon et al. 1994) and 300 pc to IC 348 (Herbig 1998, and references therein), with an error of 10% for each. The typical stellar ages in these regions have been estimated to be around 1-3 Myr (Kenyon & Hartmann 1995; Herbig 1998; Palla & Stahler 2000). There are three components to our sample:

• IC 348 core region: these objects originate from the NICMOS imaging survey of Najita et al. (2000). By using narrow-band photometry to measure the depth of the 1.9 μ m H₂O absorption band, they derived spectral types and extinctions for all objects down to K = 16.5 mag in the central $\approx 5' \times 5'$ region.² This sample of substellar objects is unique because it is complete, in the sense that every object in the survey region has an estimated spectral type. Among their identified cluster members, we observed nearly all objects with spectral types from M5.7 to M9.4, with the exception of two (objects 064-05 and 014-03, with spectral type of M5.8 and M6.3, respectively). Cluster members were selected as objects being 5 Myr or younger in their colormagnitude diagram. We also observed one object (071-01, spectral type M5.8) with an estimated age of ≈ 10 Myr. A number of these sources have published optical spectroscopy (see \S 5.1), and we have also been pursuing ground-based optical and near-IR spectroscopy (M. Liu et al., in preparation); the spectroscopy confirms that these sources are genuine very cool (late M-type) young objects. Since this NICMOS sample has been selected and analyzed in a homogeneous fashion, our analysis will often examine the properties of this sub-sample in addition to those of our sample as a whole.

- IC 348 outer region: we include additional very cool members of IC 348 from Luhman (1999), originally selected from R and I-band optical imaging. These sources lie outside the Najita et al. (2000) survey region. Luhman (1999) used far-red optical spectroscopy to derive spectral types and J-band extinctions. No errors are given for his extinction determinations; we conservatively assume these are 0.1 mag.
- Taurus: we include nearly all published objects with spectral types of M6 or later in the Taurus starforming region. These objects were originally found from optical or X-ray surveys. Four of them come from Martin et al. (2001), who derived spectral types from far-red optical spectroscopy and V-band extinctions from broad-band colors. The remaining objects have spectral types from Briceño et al. (1998) and Luhman et al. (1998a); for these, we use H-band extinctions derived by Luhman (2000) from broad-band colors. No errors are given for the published extinction determinations; we conservatively assume these are 0.5 mag and 0.1 mag for the Martin et al. (2001) and Luhman (2000) results, respectively.

Figure 1 plots our targets in comparison to theoretical models from Baraffe et al. (1998, 2002), D'Antona & Mazzitelli (1997), and Burrows et al. (1997). For the D'Antona & Mazzitelli models, we use a newer unpublished version, which we refer to as the DM98 models.³ To compare the models to the observations, we use a linear fit for the conversion between spectral type and effective temperature $(T_{\rm eff})$ advocated by Luhman (1999) for pre-main sequence objects:

$$T_{\text{eff}}(K) = 3850 - 141.0 \times SpT$$
 (1)

where SpT is the M spectral subclass, i.e., SpT = 0 means M0, SpT = 5 means M5, etc. To plot the DM98 and Burrows et al. models, we also use a linear fit to K-band bolometric corrections derived by Leggett et al. (2000, 2001):

$$BC_K = 3.99 - T_{\text{eff}}/2424$$
 . (2)

The scatter about the fit is ≈ 0.1 mag in BC_K , negligible for our purposes.

The model-derived masses range from ≈ 15 to $100 M_{Jup}$. These depend on the choice of models and temperature scale; our choices lead to conservative (i.e., larger) values

 $^{^2}$ The spectral types in the IC 348 core sample are estimated from the correlation between I-band spectral types and the strength of the 1.9 μm water band, as measured for both field dwarfs and a subsample of young stars in IC 348 itself (see Najita et al. 2000 for details). The use of fractional M subtypes reflects the continuous nature of the water index measurement and is not meant to advocate a new spectral typing convention.

The models are available at http://www.mporzio.astro.it/~dantona.

for the masses (see \S 5.5). The ages inferred from the models are \lesssim 5 Myr, and do not depend strongly on the choice of temperature scale since the isochrones are roughly horizontal in the HR diagram. Taken at face value, some models indicate that the lower mass objects tend to be younger than the higher mass ones. However, given the substantial uncertainties in the models of young substellar objects (Baraffe et al. 2002), we largely avoid using model-derived quantities in our analysis. Instead, we assume that the stars and brown dwarfs in these regions are approximately coeval, and adopt the age estimate of a few Myr derived for the stars.

2.2. L'-band Imaging: UKIRT

We obtained L'-band (3.4–4.1 μ m) imaging on 13–15 October 2001 UT at the 3.8-m United Kingdom Infrared Telescope (UKIRT). We used the facility camera IR-CAM/TUFTI, which employs a 256 \times 256 InSb array and has a pixel scale of 0″.081 pixel⁻¹. The filter used was the L'-band filter produced by the Mauna Kea Filter Consortium (3.4–4.1 μ m; Simons & Tokunaga 2001; Tokunaga et al. 2001). UKIRT has a fast-steering secondary mirror which provides tip-tilt correction by sensing a star off-axis of the science target. The typical resulting image quality was excellent (0″.35–0″.4 FWHM), and none of our sources were resolved into binaries. Conditions were photometric. During the course of the night, we regularly observed standard stars from a UKIRT in-house calibrator list.

We used a standard "two-beam" observing technique in order to accurately cancel the very large and variable thermal flux from the atmosphere. For each target, we obtained a coadded set of short integrations, then offset the telescope by about half of the array and integrated again. This was repeated, with small dithers at each nod position to ensure the object did not fall on the same position on the array. Integration times were determined using the published K-band magnitudes, spectral types, and extinctions to reach comparable S/N for all the objects. The on-source integration ranged from 3 to 60 min.

Reductions were done in standard fashion for thermal IR imaging. For each object, a flat-field was created from the average of all the images. Each flat-fielded image was then subtracted from the corresponding image in the other nod position. The images were registered using the relative telescope coordinates and averaged together. The resulting mosaic contained a positive and negative image of the target. Both were measured, and the standard error of the results was adopted as the uncertainty. For the standard stars, we used a 5" radius, as is done for the UKIRT standard star programme. We then determined a zeropoint and extinction coefficient for each night. Since most of our targets are faint, we used a smaller aperture (10 pixel radius) for their photometry, and then applied an aperture correction out to 5" based on curves of growth measured nightly from the much brighter standard stars. The size of this correction was on the order of 0.15 mags.

Table 1 presents our resulting measurements. The final errors for the object magnitudes are the quadrature sum of the errors in the raw photometry (the dominant term), the zeropoint, the extinction coefficient, the aperture correction, and the standard star magnitudes.

One object in the photometry sample, 045-02 in IC 348,

was significantly bluer in K_S-L' than the colors of late M dwarfs. Based on JHKL' colors, it is probably a background late-type giant whose position in the observed color-magnitude diagram overlaps the cluster members. We include its photometry in the Table 1, but the object is excluded from the analysis.

2.3. IR Photometry: 2MASS

We applied very small transformations to all the relevant photometry, namely the IR colors for field and young cluster M dwarfs, to bring them to a common photometric system. We chose to use the well-understood 2MASS system (Carpenter 2001). For the JHK colors of M dwarfs in the solar neighborhood, we used measurements from Leggett (1992, hereafter L92), Leggett et al. (1998, hereafter L98), and Leggett et al. (2002, hereafter L02), excluding the subdwarfs. The L92 and L98 near-IR data are on the CIT system, which we converted to the 2MASS system using Carpenter (2001). The data from L02 are on the MKO-NIR system, which we converted using additional transformations from Hawarden et al. (2001). The transformed samples showed no significant differences in their near-IR colors. For the L'-band data, all the data were either in the UKIRT system (L92 and L98 data) or the MKO-NIR system (L02 data and our observations). These are essentially identical for M dwarfs so no transformations were needed (L02).

The Najita et al. (2000) sample has been observed in the HST/NICMOS F166N and F215N filters, which are 1% bandwidth. These filters are placed in feature-free regions of H- and K-band stellar spectra. To convert these measurements to a standard photometric system, we matched 77 objects in the Najita et al. sample with objects in the 2MASS Second Incremental Data Release (Cutri et al. 2000). We found (F166N-H) = 0.00±0.02 mags and (F215N- K_S) = 0.08±0.01 mags with no statistically significant dependence on J-K color. We added J-band data from 2MASS, available for 23 out of 25 objects.

For the Luhman (1999) IC 348 sample, we used 2MASS near-IR photometry, available for all the objects except one (#405). For that one, we used his published photometry. The published near-IR photometry for the Taurus sample all came from 2MASS.

3. OBSERVATIONAL RESULTS

We identify IR excesses around our targets using K_S-L' colors, which track the shape of the SEDs from 2.0–4.1 μ m. This choice is advantageous for several reasons, including: (1) disks are more luminous at longer wavelengths, as compared to just using JHK data; (2) the effects of extinction (and uncertainties therefrom) are reduced at longer wavelengths; (3) the small wavelength range minimizes the effect of extinction errors; (4) previous studies of disks around T Tauri stars have used these wavelengths; (5) color measurements are distance independent; and (6) there is ample published K_S-L' data for field M dwarfs. Note that all the results discussed in this section are strictly empirical, e.g., independent of theoretical models and choice of temperature scale.

3.1. IR Excess Frequency and Amplitude

The top panel of Figure 2 shows our observations: $K_S - L'$ colors for the sample as a function of spectral type compared with the colors of the field M dwarf sample described in § 2.3. A substantial number of objects show $K_S - L'$ colors redder than expected from purely photospheric emission, while the lower envelope of the observed color distribution agrees well with the dwarf locus.

Since all objects in our sample have measured spectral types and extinctions, we can determine their intrinsic photospheric K_S-L' colors, and hence we are very sensitive to the presence of excess IR emission, i.e., the presence of circumstellar disks. The bottom panel of Figure 2 shows the dereddened K_S-L' colors, using the published extinctions and the extinction law from Mathis (2000). A few trends are apparent: (1) most objects have dereddened K_S-L' colors in excess of that expected from their photospheres alone; (2) the lower envelope of the color distribution is consistent with the locus of field M dwarfs, suggesting that such objects provide a legitimate comparison (see also § 5.3); and (3) the maximum amplitudes of the IR excesses decrease at later spectral types, i.e., lower masses.

For each object, we compute the intrinsic $K_S - L'$ excess in the usual fashion:

$$E(K_S - L')_0 = (K_S - L')_0^{observed} - (K_S - L')_0^{photospheric}.$$
(3)

The photospheric colors as a function of spectral type are determined from the field M dwarf sample. To compute the error in $E(K_S-L')_0$, we add in quadrature the errors in the K_S-L' colors, the reddening, and the spectral types (which add an uncertainty to the intrinsic photospheric color). The resulting excesses and their errors are listed in Table 1. In general, the excesses are much smaller than those observed for T Tauri stars (e.g. Kenyon & Hartmann 1995).

Table 2 gives the breakdown of the IR excess fraction by spectral type and target subsample. Overall, 31 out of 38 (82%) of the sample show $(K_S-L')_0$ excesses, with 21 out of 38 (55%) having excesses larger than their 1σ measurement error. To compute the disk frequency and its uncertainties, we use a Monte Carlo technique described in Appendix A which accounts for both the (gaussian) measurement errors and the (Poisson) counting errors. We find an excess frequency of $77\% \pm 15\%$ for the sample — disks around young brown dwarfs and VLM stars appear to be very common.

Next, we examine any correlations between the IR excesses and other physical properties of the objects. Note that since the detected amount of disk emission depends on the viewing angle to the observer, any such trends are not expected to be very strong. Random variations in the viewing orientation will inevitably act to obscure such trends.

3.2. Correlation with $H\alpha$

For T Tauri stars, both the optical line emission and the IR excess are believed to originate from an accretion disk. The IR excess comes from warm dust grains in the disk, while $H\alpha$ emission originates from the accretion of disk material onto the central star, e.g., via a boundary layer or a magnetically regulated accretion flow. Therefore, the $H\alpha$ emission and IR excesses should be correlated, and indeed

such a correlation is seen among T Tauri stars (e.g. Valenti et al. 1993; Kenyon & Hartmann 1995). Figure 3 shows such a comparison for our sample of young VLM stars and brown dwarfs, using H α data mostly from the literature (Briceño et al. 1998; Luhman et al. 1998a,b; Luhman 1999; Martín et al. 2001; K. Luhman 2002, priv. comm.). The entire Taurus sample has published H α measurements, and about half of the IC 348 sample does. A correlation is seen between $E(K_S-L')_0$ and H α equivalent width, with a Spearman rank correlation coefficient $r_S=0.64$. The probability of this being drawn from a random sample is 0.0009, or a 3σ correlation. This is comparable to the correlation observed for T Tauri stars (Kenyon & Hartmann 1995) and provides strong circumstantial evidence for accretion disks around young brown dwarfs.

3.3. Non-Correlations with Mass and Age

Figure 4 presents a histogram of $(K_S-L')_0$ excesses as a function of spectral type. For the three earliest spectral type bins (M5.7-M6.4, M6.5-M7.4, and M7.5-M8.4), a Kolmogorov-Smirnov (K-S) test (Press et al. 1992) finds a high probability ($\geq 40\%$) that all the samples are drawn from the same parent population. Since the evolutionary tracks at constant mass are roughly constant in $T_{\rm eff}$ for young ages, the spectral types correspond to a relative mass scale. Hence, we find no evidence for a strong dependence of IR excesses on mass. The exceptions are the coolest (lowest mass) objects, types M8.5–M9.4, where the excesses are small, consistent with non-existent. The disk frequency likewise appears to be independent of mass (Table 2), though larger samples of the coolest objects are needed to better study this issue. Using only the homogeneous IC 348 core sample gives comparable results.

In Figure 4, there is a hint that the Taurus population might tend to have larger $(K_S-L')_0$ excesses than the IC 348 samples. However, a K-S test of the M6–M7 objects shows the Taurus $(K_S-L')_0$ excess distribution differs from that of the IC 348 core sample at only the 1.5 σ level. Also it is not clear if/how the selection effects of the Taurus sample impact such a comparison. Hence, we find no strong evidence for differences in the sub-samples' IR excesses.

Figure 5 examines the age dependence of the inner disk properties by plotting the $(K_S-L')_0$ excesses as a function of dereddened absolute K_S -band magnitude, M_{K_S} . If we separate objects by spectral subclass, M_{K_S} can be used as a surrogate for age, due to the fact that model isochrones are roughly horizontal in the HR diagram. We find no statistically significant ($\gtrsim 1\sigma$) correlation between the IR excess and M_{K_S} using the Spearman rank correlation. tion test. This lack of correlation is also seen for the more homogeneous IC 348 core sample. (The exception is the M6.5-M7.5 bin, which exhibits a correlation of modest statistical significance. But this is driven by the one Taurus object with a very large $E(K_S-L')_0$. When this object is excluded, the correlation disappears.) If we adopt an age for the substellar population based on that estimated for the stars (see § 2.1), our findings suggests that the inner regions ($\leq 0.1 \text{ AU}$) of young brown dwarf disks do not evolve substantially over the first ~ 3 Myr. This timescale is in accord with studies of disks around T Tauri stars (e.g. Strom et al. 1989; Skrutskie et al. 1990).

4. ANALYSIS OF DISK PROPERTIES

4.1. Disk Models

We use simple models of circumstellar disks to examine the observed infrared excesses. Our goal here is not to deduce detailed physical properties, but to understand the general characteristics and trends of our observations. For simplicity, we assume that the disks are optically thick and geometrically flat. Similar models have been widely used to understand the emission from disks around the higher mass T Tauri stars (e.g. Lynden-Bell & Pringle 1974; Adams et al. 1987; Lada & Adams 1992; Hartmann 1998, and references therein). The assumption of a flat disk is appropriate for the inner disk region from which the K_S-L' emission originates. Although in reality disks probably flare significantly at larger radii, the impact of the flaring on the SED is much more important at mid-IR $(\sim 10 \ \mu \text{m})$ and longer wavelengths (e.g. Kenvon & Hartmann 1987; Wood et al. 2002). Indeed there are some indications from mid-IR measurements that flat disks might be more appropriate for some young brown dwarfs (Natta et al. 2002).

For both active accretion and passive reprocessing of stellar irradiation, the disk temperature profile follows $T \propto r^{-3/4}$, where r is the radial position in the disk. The normalization of the temperature profile is determined from the total luminosity that is produced by reprocessing and accretion. (The heating of the star by radiation from disk is ignored.) For a disk that extends from an infinite outer radius to an inner radius R_{in} , the luminosity from reprocessing is

$$L_{rep} = 0.25 \left(\frac{R_*}{R_{in}}\right) L_* \tag{4}$$

where L_* and R_* are the luminosity and radius of the central source, respectively (Adams & Shu 1986). For the same disk, the luminosity from accretion is given by

$$L_{acc} = \frac{GM_*\dot{M}}{2R_{in}} , \qquad (5)$$

where M_* is the mass of the central source and \dot{M} is the disk accretion rate. Half of the total potential energy of the accreting material is radiated away, with the other half stored as rotational energy. In principle, the accretion luminosity can become arbitrarily large, since it scales with \dot{M} , in contrast to the reprocessing luminosity which has a maximum of $0.25L_*$. In practice, for typical T Tauri stars, the luminosity in excess of the stellar photospheres is $\approx 0.25L_*$, i.e., about the maximum expected from a flat reprocessing disk alone (Hartmann 1998).

Given the contributions from reprocessing and accretion, we compute the resulting disk SED by summing over annuli, assuming each annulus radiates as a blackbody. To compute broad-band magnitudes from the resulting model SEDs, we use transmission profiles which account for the combined spectral response of the detector, filter, and atmosphere. We obtained JHK_S profiles from 2MASS, and L'M' ones for the MKO system from UKIRT (S. Leggett, priv. comm.). In computing the emergent flux from the star+disk spectrum, we account for the non-blackbody nature of the stellar spectra, a small, but noticeable, effect for cool M-type photospheres. We adjust the stellar spectra in the models to match the IR color locus for field M dwarfs

described in § 2.3. In doing so, we make use of bolometric corrections computed by Leggett et al. (2000, 2001). Although we have ignored, for simplicity, the true non-blackbody nature of the disk emission (e.g. Calvet et al. 1992), we note that the results of these simple models agree well with those of Calvet et al. as presented in Meyer et al. (1997) for the low accretion rates considered here.

Table 3 tabulates the maximum possible excess from our reprocessing disks, i.e., for a face-on orientation with no inner hole. Figure 6 shows the resulting JHK_SL' colorcolor diagram for stars with reprocessing disks for a range of central stars, viewing angles, and hole sizes. The resulting models all have roughly the same color-color slope. The plotted stellar loci for giant and dwarf stars are from Bessell & Brett (1988), converted to the 2MASS system. We use 2nd order polynomial fits to represent the mean colors of M1 to M9.5 dwarfs, based on Leggett (1992), Leggett et al. (1998), and Leggett et al. (2002) data; the rms scatter about the fit is consistent with the measurement errors. We adopt the reddening law from Mathis (2000) for $R_V = 3.1$. Notice that (1) the disks around earlier type (hotter, more luminous) objects generate much larger IR excesses than those around later type (cooler, less luminous) objects; (2) mid-M type objects (near the stellar/substellar boundary) with disks are predicted to be bluer in J-H than either early-M types (representative of T Tauri stars) or late-M (substellar) objects with disks; and (3) models with significant holes generate color excesses in only K_S-L' , because the inner disk regions are relatively cool.

4.2. Evidence for Inner Disk Holes

L'-band observations are sensitive to emission from the hot, inner portions of circumstellar disks. For the range of $T_{\rm eff}$ considered here, the emission comes from a region within a few radii of the central source ($\lesssim 0.1 \text{ AU}$). Hence, the presence of inner holes in the disks will have a substantial impact on the K_S-L' emission. Disks with inner holes of a few stellar radii have been inferred to exist around the higher mass T Tauri stars (e.g. Kenyon et al. 1996; Meyer et al. 1997) and are believed to originate from the interaction of the stellar magnetic field with the accretion disk (e.g. Bertout et al. 1988; Königl 1991; Shu et al. 1994). Modeling and interpreting the disk emission from a specific object depends on the viewing angle to the observer, which is unknown. This limitation can be overcome with a large unbiased sample of objects, as is the case for our study — meaningful constraints on the inner holes can then be found from (1) the maximum observed IR excess and (2) the observed distribution of IR excesses.

Figure 7 illustrates the effect of inner holes on passive disk models viewed face-on. Holes of $\gtrsim 4R_{\star}$ are sufficient to quench any K_S-L' excess, especially for later-type (cooler) objects. One interesting aspect of Figure 7 is that none of our targets are observed to have an IR excess as large as the model without an inner hole $(R_{in} = R_{*})$. The observed upper envelope is more consistent with the $R_{in} \approx 2-3R_{\star}$ models, suggesting inner holes are common. Note that for a specified hole size, the distribution of excesses should peak near the maximum excess based on simple geometrical considerations. The probability distribution of viewing angles follows $P(\theta) = \sin \theta$. Although

disks seen nearly face-on ($\theta \sim 0^{\circ}$) are rare, the decrease of disk flux with $\cos \theta$ compensates for this. The net result is that the color distribution in magnitudes for a random population of disks is strongly peaked towards the maximum excesses (e.g. Kenyon & Hartmann 1990).

To quantitatively examine the possibility of inner holes, we compare the observed $E(K_S-L')_0$ color distribution against Monte Carlo realizations of star+disk models viewed at randomly selected viewing angles. We first construct a series of passive disk models with a fixed inner radius. The amplitude of the IR excess depends on the viewing angle θ and the $T_{\rm eff}$ of the central source: hotter stars with disks can produce larger IR excesses than cooler stars with disks. However for the range of temperatures considered here, the $T_{\rm eff}$ dependence is removed when the model excesses are normalized against the maximum possible excess (i.e., $\theta = 0^{\circ}$). This normalization allows us to examine models which depend only on the viewing angle, which are needed to compare with the Monte Carlo simulations. Thus, for each object, we compute the normalized excess, defined as

$$\mathcal{E}(K_S - L')_0 = \frac{E_{K_S - L'}^{obs}}{\max(E_{K_S - L'}^{model})}$$
(6)

where the numerator is the observed $(K_S - L')_0$ excess and the denominator is the $K_S - L'$ excess from a face-on passive disk model computed for the T_{eff} corresponding to the object's spectral type. $\mathcal{E}(K_S - L')_0$ is simply the ratio of the observed excess to the maximum possible model excess.

We exclude objects with small observed $E(K_S-L')_0$ from this analysis; these objects would correspond to model disks viewed nearly edge-on. In such cases, the disk probably obscures the central source, and hence these objects are missing from the original imaging surveys. Objects in our sample with small $E(K_S-L')_0$ are probably not those with disks viewed nearly edge-on, but rather objects without significant disks. We choose a cutoff value of $\theta=80^{\circ}$, corresponding to a 100 AU flared disk with an outer height of 17 AU; this agrees well with results from HST imaging of the edge-on Taurus object HH 30 (Burrows et al. 1996).

For a given inner hole radius, we compare the observed $\mathcal{E}(K_S-L')_0$ distribution with that expected from a Monte Carlo set of disks chosen with random viewing angles. The results are shown in Figure 8 for models with inner disk radii of 1, 2, and $3R_{\star}$. Models without inner holes predict many more objects with large values of $\mathcal{E}(K_S-L')_0$ than observed; this is equivalent to the findings in Figure 7, where there are no objects with excesses as large as the face-on models without holes. On the other hand, models with inner radii of $3R_{\star}$ predict much smaller excesses than observed. Only models with inner radii of $\approx 2R_{\star}$ agree well with the data. This is confirmed using the K-S test: for a hole radius of $2.2R_{\star}$, the K-S test indicates a 82% chance that the observed and the predicted $\mathcal{E}(K_S-L')_0$ distributions originate from the same population. This is much better concordance than for the $1R_{\star}$ and $3R_{\star}$ hole models; the K-S test indicates a \gtrsim 1000× lower probability of these models being drawn from the same parent population as the observations.

To summarize, we find the observed maximum amplitude and color distribution of the $(K_S - L')_0$ excesses point

to disks with characteristic inner radii of $\approx 2R_{\star}$. Note that our analysis based on passive disks provides a lower estimate of the hole size: larger holes could be accommodated if the luminosity from accretion is substantial (see § 4.3) or if the vertical flaring of the disks is unexpectedly large. Mid-IR observations of young brown dwarfs in ρ Oph may also suggest the presence of inner holes (Natta et al. 2002). Finally, as illustrated in Figure 7, holes of $\gtrsim 2R_{\star}$ could account for the small/negligible IR excesses observed for the M9 sources in our sample. Longer wavelength data are need to conclusively determine whether these very cool objects have disks.

4.3. Constraints on Accretion Rates

The widespread presence of $H\alpha$ emission among the sample (§ 3.2) indicates that accretion is ongoing for most objects. To roughly constrain the accretion rate, we rearrange equations (4) and (5) to compare the relative contributions of reprocessing and accretion luminosity for the case of a simple flat accretion disk:

$$\frac{L_{acc}}{L_{rep}} = 0.3 \left(\frac{\dot{M}}{10^{-9} M_{\odot}/\text{yr}} \right) \left(\frac{M_{BD}}{60 M_{Jup}} \right) \times \left(\frac{L_{BD}}{0.02 L_{\odot}} \right)^{-1} \left(\frac{R_{BD}}{0.6 R_{\odot}} \right)^{-1} \tag{7}$$

where we have used values for the mass, luminosity and radius representative of our sample. As discussed in the previous section, the magnitude of the observed IR excesses can be generated by a reprocessing disk alone. There is no need to invoke significant luminosity from mass accretion, which suggests accretion rates are $\lesssim 10^{-9}~M_{\odot}~\rm yr^{-1}$. Such rates are comparable to the lowest accretion rates measured for classical T Tauri stars (CTTS); typical CTTS rates are around 10^{-7} to $10^{-8}~M_{\odot}~\rm yr^{-1}$ (e.g. Valenti et al. 1993; Gullbring et al. 1998). Such low rates also indicate that young brown dwarfs accumulate at most $\sim 10\%$ of their final mass via disk accretion, if the current rates are representative of their time-averaged accretion history.

For one of our targets, the M6 object V410 Anon 13 in Taurus, Muzerolle et al. (2000) find its H α line profile is well-fitted using magnetospheric accretion models in which the magnetosphere extends to $2.2-3R_{\star}$, in accord with our analysis of the $(K_S-L')_0$ excesses in the previous section. They derive an accretion rate of $\sim 5 \times 10^{-12} M_{\odot} \text{ yr}^{-1}$, well below our estimated upper limit. More such direct measurements for young brown dwarfs are sorely needed to determine the typical accretion rate and its dispersion.

As mentioned before, there is a degeneracy in determining the inner hole size and the accretion rate based on the IR data alone. Pure reprocessing disks with $\approx 2R_{\star}$ inner holes can account for the observed IR excesses (§ 4.2). But disks with larger inner holes can also agree with the data if the accretion rates are significant. For instance, disk models with $3R_{\star}$ holes and accretion rates of $\sim 10^{-9}~M_{\odot}~\rm yr^{-1}$ can generate comparable excesses. However, such accretion rates would disagree with H α measurements of young brown dwarfs by Muzerolle et al. (2000, 2002), which include a few objects common to our L'-band sample. Even larger inner holes of $4-5R_{\star}$ would make reprocessing nearly irrelevant (e.g., Figure 7), and the accretion rates required to generate the observed excesses ($\gtrsim 10^{-8}~M_{\odot}~\rm yr^{-1}$) would be even more discrepant.

Thus it is unlikely that the characteristic sizes of the inner holes are much larger than $\approx 2R_{\star}$.

5. POTENTIAL SYSTEMATIC EFFECTS

Our identification and analysis of IR excesses depend on several measurements which may be prone to systematic errors. Here, we find that they should not have a significant impact.

5.1. Extinctions and Spectral Types

Measuring the IR excesses depends on the adopted spectral types and extinctions. As a check on these, we examine the subset of our IC 348 core sample which has been studied by more than one group. Twelve of the objects, about half the sample, have been classified using both IR narrow-band spectrophotometry (Najita et al. 2000) and optical/far-red spectroscopy (Luhman 1999); these twelve are roughly distributed across our sample's full range of spectral types. The K-band extinctions measured by the two studies agree well, with a median difference of 0.03 mag and an rms of 0.12 mag. This concurs with the analysis of Najita et al. for their entire IC 348 sample. Note that since we are measuring IR color excesses, we are somewhat less sensitive to errors in A_K than if we were simply measuring bandpass magnitudes.

As for the spectral types, the Luhman spectral types tend to be ≈ 1 subclass earlier than those of Najita et al. This is expected, given the spectral type calibration chosen by Najita et al. (see their Figure 7, bottom panel). If the Luhman (1999) types are adopted, the net result is that the IR excesses we measure would be larger, strengthening our finding that IR excesses are common in this sample. Of course, the mass estimates would be increased, pushing some objects from brown dwarf to VLM stars, but this would not change our findings about the high frequency of IR excesses in this very low mass sample. Likewise, our analysis of the inner hole sizes (§ 4.2) would not be impacted much, since the maximum $E(K_S-L')_0$ for the models has only a weak dependence on spectral type for M5 to M9 objects (Figure 7). Hence, the uncertainties in the spectral types and extinctions do not seriously affect our analysis.

5.2. Contamination from Disk Emission

Disk emission can in principal lead to systematic errors in the derived spectral types and extinctions. This is unlikely to be an issue for the Taurus and IC 348 outer samples, since the spectral typing was done at optical wavelengths (*I*-band) where any disk emission should be negligible. However, disk emission contamination is potentially more important for the IC 348 core sample, whose spectral types are based on NICMOS 1.6–2.2 μ m narrow-band photometry measuring the 1.9 μ m H₂O absorption band. In a standard passive and/or accretion disk where the flux excess follows the form $\Delta F_{\lambda} \propto \lambda^{-4/3}$, disk emission would lead to weaker H₂O absorption, and hence earlier spectral types.

We use our passive disk models to quantify the impact of disk emission on the NICMOS spectral types. We explore the worst-case scenario, in which the disks do not have inner holes and hence the disk emission is maximized. Our approach is as follows: for each object, we construct passive disk models based on the measured spectral type and spanning a wide range of viewing angle θ . We use the observed $E(K_S-L')_0$ to assign a corresponding value of θ and then determine the amount of disk excess in the NICMOS narrow-band filters. Employing the Najita et al. calibration of NICMOS photometry to spectral type, we then determine the change in typing. (For a fully consistent analysis, we would do this iteratively, using the inferred error in spectral type to recompute the observed $E(K_S-L')_0$, and then repeating the above process to redetermine the systematic error in spectral type. In practice, this is unnecessary since the disk contamination is small.)

For the IC 348 core sample, we find the median effect of contamination by disk emission is 0.2 subclasses, i.e., the objects should be classified as slightly later types. The median excess in the K-band photometry is 0.07 mags. As expected, the objects with the most significant disk contamination are those with the earliest spectral types and largest $E(K_S-L')_0$: here, the effect of disk emission can be as large as $\approx 0.5 - 0.7$ subclasses, producing a K-band excess of $\approx 0.2 - 0.3$ mags. Even in these cases, the consequences are minor: the effect of a later spectral type is to reduce the measured $E(K_S-L')_0$. However, the actual impact is small since the photospheric K_S-L' color changes slowly with spectral type for late M-dwarfs. Therefore, we conclude that the contamination from disk emission is not significant. In a similar vein, the impact of disk emission on the extinctions derived by Najita et al. (2000) is small.

Again, since these calculations use models without inner holes, the above results present the worst case scenario for disk contamination. In the event that the disks have inner holes of radii $\gtrsim 2R_{\star}$, as we infer in § 4.2, the effect of disk emission on the NICMOS-derived spectral types and extinctions is negligible.

5.3. Surface Gravity

We have used the colors of field M dwarfs in order to identify which of our targets have intrinsic IR excesses. However, our targets are pre-main sequence objects, and hence will have lower surface gravities than the field M dwarfs. The sense of this effect is likely that at objects with lower gravities have bluer $K_S - L'$ colors. This is seen in Figure 6, where the $K_S - L'$ colors of giant stars (spectral types G0 III to M5 III) are comparable to or bluer than dwarf stars (A0 V to M9.5 V). Pre-main sequence stars are intermediate in surface gravity, and hence we expect their $K_S - L'$ colors to be no redder than the dwarf stars. If they are bluer than dwarfs, then we would infer that the IR excesses are larger and even more common.

Given the current uncertainties in the theoretical atmospheres, we chose not to use the models to measure $E(K_S-L')_0$ in § 3, but instead used the empirical field dwarf locus. Here, we examine the Baraffe et al. (1998, 2002) models to explore the *relative* shift in color due to gravity effects. Figure 9 plots models with ages of 1 Myr and 1 Gyr: there is a difference of a factor of ≈ 30 in the surface gravities at fixed mass. The $T_{\rm eff}$ for the older (1 Gyr) models have been converted to spectral type using results for field M dwarfs from Leggett et al. (2000, 2001) and Tsuji et al. (1996), fitted to a linear relation:

$$T_{\text{eff}}(K) = 3851 - 185.3 \times SpT,$$
 (8)

where SpT is the M spectral subclass. For the younger (1 Myr) models we use either this scale or the aforementioned Luhman (1999) scale (equation (1)). Both the "clear" and the "dusty" atmospheric models predict that younger, lower gravity objects have bluer colors at fixed spectral type. The amplitude of the difference varies with the choice of model and temperature scale, but generally lower gravity objects are predicted to be 0.1 mag bluer in $K_S - L'$ at fixed spectral type.

Perhaps the most convincing evidence that gravity effects do not significantly affect the photospheric colors can be seen in the data themselves. The loci of the observed and dereddened K_S-L' colors in Figure 2 both show a lower envelope which agrees well with the empirical dwarf locus, to better than $\lesssim 0.05$ mag. This level of difference has little bearing on our analysis.⁴

5.4. Sample Selection Biases

Biases in the sample selection could impact our conclusions. For example, if brown dwarfs without disks are systematically excluded from our sample, then our estimate of the disk-bearing fraction will be incorrect. The effect of extinction on the sample selection is probably the primary concern. Objects with edge-on disks will be heavily extincted and are almost certainly missing from the optical/IR imaging surveys used to construct our sample. (Indeed, this bias is also present in most previous T Tauri disk studies using broad-band photometry.) Viewing angles of greater than 80°, which is the cutoff value we adopt in $\S 4.2$ for obscured edge-on disks, account for 17\% of a random distribution of disk inclinations, so the disk fraction for our sample would be underestimated by only a small amount ($\approx 3\%$). Also, including such objects would only act to increase the measured disk fraction, which we already find is very high.

One common approach to minimizing selection biases is to use a complete sample, where all the objects in a given area on the sky are identified to a well-defined limit. The Najita et al. (2000) survey is the source of our IC 348 core sample; this survey is K-band selected and has a welldefined completeness limit for spectral classification. We have L'-band observations for nearly every cluster member from their survey in the M5.7 to M9.4 range; only 2 objects out of 26 were not observed. Also, most of our targets are several magnitudes brighter in K-band than the survey limit. Therefore, we expect that our IC 348 core sample is essentially complete, and that selection biases due to extinction are negligible. The trends we identified in § 3 for our entire L'-band sample are also found if we consider only the IC 348 core sample. This suggests that selection biases are probably not a significant effect when analyzing the L'-band sample as a whole.

The three coolest/lowest mass objects, all with spectral type \approx M9, have negligible IR excesses. This might be due to a selection effect if objects with larger excesses tended to be preferentially extincted and hence missing

from the sample. But there is no evidence for this effect: for the M5.7 to M7.7 objects, no statistically significant ($\gtrsim 1\sigma$) correlation exists between $E(K_S-L')_0$ and A_K . Also, even the M9 objects are 1.5 mags above the K-band survey limit of Najita et al. Thus, it is unlikely there are M9 objects with large excesses which are missing from our sample because of large extinctions. However, a much larger sample of M9 (and cooler) sources are needed to accrurately assess the disk fraction of such low mass objects ($\lesssim 15-20~M_{Jup}$).

5.5. Pre-Main Sequence Temperature Scale and Mass Estimates

When analyzing the trends in the disk properties (§ 3), we used the observable quantities of spectral type and M_{K_S} as surrogates for the relative masses and ages of the targets. Preferably, one would like to use absolute values for masses and ages, as obtained from theoretical models. However, an examination of Figure 1 shows the problem: different models give very different results. Also, the current models do not always cover the observed location of the young brown dwarfs in the plot. (This is true using either K-band absolute magnitude or bolometric magnitude as the ordinate.)

An important caveat is the choice of the conversion between $T_{\rm eff}$ and spectral type. We have used the Luhman (1999) scale throughout. If we had used a scale appropriate for field M dwarfs (equation (8)) then evolutionary models of a given temperature would correspond to earlier spectral types — the net result would be much lower mass estimates for our targets, with masses of $\lesssim 10~M_{Jup}$ for the coolest ones. Hence our choice of the Luhman (1999) scale is a conservative one. Similarly, the disk modeling results in Table 3 would change by ≤ 0.05 mag with a dwarf temperature scale, and our other analyses using disk models in \S 4 would also be unaffected.

We reiterate that our targets are selected based on their spectral types. The resulting sample is significantly cooler than previous L-band surveys, which were sensitive down to spectral types of $\sim \!\! \text{M5}$ (Kenyon & Hartmann 1995; Haisch et al. 2001a), and hence comprise the lowest mass sample of young objects studied to date at these wavelengths, independent of the choice of temperature scale.

6. DISCUSSION

6.1. Disk Frequency of Young Stars and Brown Dwarfs

In our sample of brown dwarfs and VLM stars, we find 31 out of 38 objects possess intrinsic IR excesses (82% \pm 15%, where we quote only Poisson statistical errors in this section in order to compare with previously published results). This disk fraction is comparable to, or exceeds, the disk fraction for the higher mass stars in the same star-forming regions. Using multi-band photometry and spectral types, Strom et al. (1989) found 47 out of 83 (57% \pm 8%) T Tauri stars in Taurus have significant K-band excesses ($\Delta K \geq 0.1$ mag). (See also Kenyon &

⁴ One interesting feature is that the dusty models predict fairly constant K-L' colors for objects with mid to late-M type objects, especially when using the Luhman (1999) temperature scale. This is inconsistent with the observations. For field M6–M9 dwarfs, the models are $\approx 0.1-0.2$ mag bluer than the observed colors (e.g., the solid line plotted in Figure 2). Likewise, the dusty models have bluer K_S-L' colors than the observed lower envelope for our sample of young M dwarfs (Figure 2). However, our sample contains only a few young M9 objects, so the observations would allow for constant K-L' colors if this effect in fact begins around M8, instead of at M6 as currently predicted by the dusty models. If this is the case, then the M9 objects would have actually small IR excesses, whereas they are currently inferred to have almost none.

Hartmann 1995.) Haisch et al. (2001a) found a similar disk fraction of $65\% \pm 8\%$ for stars in IC 348. Some caution is in order when comparing our IC 348 results with those of Haisch et al. The latter used only multi-band photometry without spectral type information, and hence, as we discuss below, their disk fraction may be somewhat underestimated.

The most common method for measuring the disk fraction of young stars uses color-color diagrams based on JHK, or preferably JHKL, colors. Objects with disks are identified as those having IR colors distinct from reddened dwarf and giant stars. This method has been used extensively to study the frequency, properties, and evolution of circumstellar disks around T Tauri stars (e.g. Lada & Adams 1992; Kenyon & Hartmann 1995; Lada & Lada 1995; Meyer et al. 1997; Haisch et al. 2001b). The method is appealing since only photometry is used, without need for more time-consuming spectroscopy. Moreover, the method has been demonstrated to be effective for T Tauri stars, e.g., Hillenbrand et al. (1998) and Haisch et al. (2001c) show that most TTS in Taurus with multiwavelength evidence for disks can be identified from JHK colors alone, and all can be found with JHKL colors. Here we consider the value of this method for studying disks around young brown dwarfs.

Figure 10 illustrates the commonly used IR color-color analysis applied to our sample. From this diagram, one would identify only 11 out of 36 objects as having IR excesses. (Two objects do not have 2MASS J-band photometry.) However, our analysis which incorporates the objects' spectral types and extinctions shows that in fact many more objects (31 out of 36) have IR excesses. The majority of sources with disks are missed in the color-color diagram because their IR excesses are modest. In fact, an analysis using only JHK_S colors, without L'-band data, would find only 2 out of 36 objects with IR excesses, i.e., essentially missing all the objects with disks. These observational results confirm model predictions of very small JHK excesses from brown dwarf disks (e.g., Natta & Testi 2001, this work).

There are two physical reasons why using only IR colors works poorly. Both lead to decreased contrast between brown dwarfs and their disks. (1) Because brown dwarfs are less luminous than the higher mass T Tauri stars, disks around brown dwarfs will be cooler and less luminous; therefore, the corresponding IR excesses will be smaller (e.g., Table 3). (2) T Tauri stars span a limited range in photospheric K_S-L' color, and hence even a modest disk excess will produce IR colors readily distinguishable in color-color diagrams. In contrast, young brown dwarfs, with spectral types of M6 and later, have redder photospheres and span a larger range in intrinsic K_S-L' color (e.g., Figure 6). Hence, the modest IR excesses produced by their disks will be harder to distinguish than for the case of T Tauri stars.

This latter item raises the fact that color-color analyses inevitably underestimate the disk fraction. Near-IR imaging samples will include objects with a range of spectral types. Earlier-type (hotter) stars with small IR excesses will not be as readily identified as disk-bearing in color-color diagrams compared to stars with larger excesses or later-type (cooler) objects which lie close to the reddening

boundary. This effect leads to an underestimate of the disk fraction. It is unlikely to be an significant error in surveys of T Tauri or Herbig Ae/Be stars, since they have a small range in intrinsic IR colors. It will be a more serious effect for young brown dwarfs.

In a similar vein, the disk fractions inferred from colorcolor analyses are very sensitive to the assumed boundary of the reddened stellar locus (the rightmost line in Figure 10). The boundary is determined by the colors of the latest spectral type objects. However, since spectroscopy is generally not available in these studies, this boundary must be estimated, which can produce either an underestimate or overestimate of the true disk fraction. Since nearly all such surveys are magnitude-limited, this systematic error can be aggravated by the variable amounts of extinction to different sample members and hence an ill-defined spectral type boundary.

Our approach of examining a sample of objects with spectral type determinations is far more sensitive to disk emission than searches based on JHK(L) photometry alone. Indeed, our results suggest that both L'-band data and spectral types are required in order for an accurate ground-based census of disks around young brown dwarfs.

6.2. Comparison with Near-IR Surveys of Trapezium and σ Ori

Two recent surveys have addressed the topic of disks around young VLM stars and brown dwarfs using large samples in Orion. Here we compare their findings with our own results.

Muench et al. (2001) have studied the disk fraction for young brown dwarfs in the Trapezium cluster using $J\!H\!K$ imaging. They select a large sample (109 objects) of brown dwarf candidates identified from their (J-H,H) color-magnitude diagram in conjunction with a 1 Myr theoretical model from Baraffe et al. (1998). Then they use $J\!H\!K$ color-color diagrams to infer a disk fraction of $\sim 65\% \pm 15\%$. Many of their objects with IR excesses clearly possess disks, because they are coincident with "proplyd" sources seen in $H\!S\!T$ optical images.

Interpreting their results is complicated by the uncertain masses of their candidates. Contamination from background stars is predicted to be low for the Muench et al. magnitude limits (e.g. Hillenbrand & Carpenter 2000), so most of the objects probably are cluster members. But brown dwarf selection from the IR color-magnitude diagram is clearly not robust: about 15% of their candidates have JHK colors consistent with reddened stars of spectral types M0 or earlier. Moreover, there is a puzzling inconsistency in the photometric selection when compared to the available spectroscopy. Ten sources in the Muench et al. survey have spectral types of M6 or later as measured by Hillenbrand (1997), indicating that they are near or below the substellar limit. However, all of these are brighter than the 1 Myr model predictions for a 0.08 M_{\odot} object, some by several magnitudes. The evolutionary models would thus indicate that these objects have stellar masses based on their brightnesses and are not brown dwarfs. Finally, the Muench et al. selection approach essentially uses unextincted J-band magnitudes, and therefore depends on the assumed age of the Trapezium cluster. Objects older than 1 Myr, and hence higher mass, might be included in the sample. For example, for an assumed age of 3 Myr, the brightest candidates would correspond to a mass of 0.15 M_{\odot} based on the Baraffe et al. (1998) models. Spectroscopic follow-up will be important for refining the mass estimates of their brown dwarf candidates.

The location of the Muench et al. Trapezium brown dwarf candidates in the JHK color-color diagram is intriguing in light of our modeling results. (1) Many of the objects exhibit H-K excesses of several tenths of a mag, substantially larger than the maximum excess predicted by simple flat disk models (Table 3). One possible explanation is that these are flared disks seen close to edge-on; models which include the effects of scattering show that such disks tend to have redder colors than simple flat reprocessing disks (Wood et al. 2002). If this is the case, the central sources will be more heavily extincted, and since the target selection was based on magnitudes, will tend to have higher masses. Another possibility is that accretion luminosity is a significant component of the disk emission, i.e., $\dot{M} \gtrsim 10^{-9}~M_{\odot}~{\rm yr}^{-1}$ (equation (7)). In this case, the implication would be much higher accretion rates for the Trapezium sample compared to the Taurus and IC 348 objects in our sample, perhaps a reflection of Trapezium's younger age and/or higher stellar density. (2) Most of the Trapezium IR excess sources lie below the CTTS locus of Meyer et al. (1997), namely they have bluer (J-H) colors. Simple disk models can explain some of the objects as being mid-M type objects with disks, which will have bluer J-H colors than the early-M type objects used to define the CTTS locus (e.g., Figure 6). However, these models cannot explain sources with very blue colors $(J-H \lesssim 0.6)$ mag). Muench et al. point out that half of these are associated with proplyds and hence are genuine disk-bearing sources; perhaps their blue colors arise from scattering. The nature of the remaining blue sources remains unresolved.

Oliveira et al. (2002) have studied the disk fraction for low mass stars and a few brown dwarf candidates in the σ Ori cluster. For a sample of 34 cluster members selected on the basis of optical photometry and Li absorption, they found at most 2 out of 34 (6% \pm 4%) objects had IR excesses, based on *JHK* colors. Adopting a cluster age of \sim 2–7 Myr, Oliveira et al. suggest that disks around very low mass objects can dissipate within a few Myr. These conclusions are cast into doubt by our results. We have shown that *JHK* colors are poor diagnostics of disks around VLM stars and brown dwarfs. Longer wavelength observations, at least in the *L*-band, are needed to measure the true disk fraction and its implications for the evolutionary time scale of disks around very low mass objects.

6.3. Properties of Young Brown Dwarfs and their Circum(sub)stellar Disks

Our results suggest that much of the observational paradigm developed for disks around T Tauri stars can be extended to disks around young brown dwarfs. Most of our sample show both IR excesses and strong ${\rm H}\alpha$ emission, like the higher mass classical T Tauri stars. Some

objects have little/no IR excesses and little $H\alpha$ emission, analogous to weak-line T Tauri stars. A few have IR excesses but only weak $H\alpha$ emission; such a phenomenon is also seen among weak-line T Tauri stars (e.g. Strom et al. 1989; Skrutskie et al. 1990; Preibisch & Zinnecker 2002). In addition, the widespread presence of $H\alpha$ emission suggests that most brown dwarfs are accreting, although the inferred rates are much lower than classical T Tauri stars.

We have also found evidence that young brown dwarfs, like their more massive counterparts, the T Tauri stars, possess circumstellar disks with inner holes (§ 4.2). What is the origin of these holes? In the case of T Tauri stars, inner holes are believed to be created through the truncation of the disk by strong, closed stellar magnetic fields; disk matter may reach the star by accretion along these stellar magnetic field lines (e.g. Bertout et al. 1988; Königl 1991; Hartmann et al. 1994; Shu et al. 1994). A similar situation may be relevant to young brown dwarfs. Like their more massive counterparts, young brown dwarfs also show signs of surface magnetic activity. For example, young brown dwarfs have detectable X-ray emission that is characterized by plasma temperatures of $\sim\!\!1\!-\!2$ keV and X-ray luminosities that are $\sim10^{-4}$ to 10^{-3} times the bolometric luminosity. The X-ray emission also displays moderate time variability and rapid flaring (Imanishi et al. 2001; Preibisch & Zinnecker 2001, 2002). These similarities strongly suggest that young brown dwarfs have significant magnetic fields.⁵

The likely disk accretion rates of the brown dwarfs in our survey are expected to be small ($\S 4.3$) and only modest magnetic fields are needed to produce the inner holes with radii of $2-3 R_*$. For example, with typical parameters of $M_* = 0.06~M_{\odot}$, $R_* = 0.6~R_{\odot}$, and a disk accretion rate of $10^{-10}~M_{\odot}~{\rm yr}^{-1}$, the required field strengths are $\sim 110 - 220$ G if the X-wind theory of Shu et al. (1994, equation 2.6b with $\alpha_X = 1$) is applied directly to this case (see also Ostriker & Shu 1995 who recommend $\alpha_X = 0.923$). This estimate assumes that the magnetosphere is only partially filled, with the accretion rate onto the star restricted to stellar loops that correspond to $\sim 10\%$ of a filled magnetosphere (Calvet & Gullbring 1998; Muzerolle et al. 2000). For comparison, the formulation given by Königl (1991) when applied directly to this case requires field strengths of $\sim 450-900$ G. These field strengths are quite modest, less than those measured for pre-mainsequence stars (Guenther et al. 1999; Johns-Krull et al. 1999a,b) and dMe stars (e.g. Johns-Krull & Valenti 1996).

It is interesting that the temperature at an inner disk radius of $2R_*$ in our disk models is approximately 1200 K, very similar to the estimated temperature for the inner disk radii of T Tauri stars (e.g. Shu et al. 1994). At the densities of inner disks and temperatures of $\gtrsim 1000$ K, thermal ionization (of Na and K) can maintain an ionization fraction that enables magnetic coupling between the star (or brown dwarf) and the disk (Umebayashi & Nakano 1988; Fromang et al. 2002). Therefore, the inner regions of brown dwarf disks will be sufficiently ionized for magnetic fields to couple to and truncate the disk at $\approx 2R_{\star}$.

⁵ This evidence for strong magnetic activity among young brown dwarfs contrasts strongly with the evidence for decreased magnetic activity among dwarfs at the bottom of the main sequence (Gizis et al. 2000). This is likely due to the higher temperatures of young brown dwarfs (i.e., spectral types of mid-M and later), which are high enough to support a partially ionized atmosphere, and therefore, surface magnetic fields, chromospheres, and coronae (e.g. Preibisch & Zinnecker 2002).

6.4. Implications for Brown Dwarf Formation

For a star like the Sun, significant disk accretion is an imperative because the angular momentum of the parent cloud core is typically too large for the star to accrete more than a few percent of its final mass through direct infall (e.g. Shu et al. 1993). If Sun-like stars and brown dwarfs form under similar initial conditions (e.g., they form from similar cloud cores), then the need for significant disk accretion is much reduced since brown dwarfs may be able to accrete a substantial fraction of their final mass through direct infall. Our results indicate that if brown dwarfs form through such means then disks are produced. In such a scenario, an important question is what determines the final mass of the object, i.e., why a given core would create a brown dwarf rather than a Sun-like star.

One physical effect which may address this concern is the premature truncation of accretion due to strong dynamical interactions at early times. Reipurth & Clarke (2001) have proposed that brown dwarfs originate as stellar embryos in small multiple systems which are prematurely ejected. These embryos accrete from a common infalling envelope, but dynamical interactions among them lead to the preferential ejection of the lowest mass members. Here, the final masses of the ejected objects are established by the termination of accretion at the time of ejection. (Note that although their work focuses on brown dwarfs, there is no clear distinction across the substellar boundary and hence this scenario might also apply to VLM stars.) The process is purported to occur at very young ages ($\sim 10^4$ yr), due to the short crossing times of the multiple systems. Preliminary studies of young star-forming regions do not find any obvious kinematic difference between the brown dwarfs and T Tauri stars (Joergens & Guenther 2001), as might be expected from preferential ejection of the young brown dwarfs. However, Reipurth et al. (2001) suggest that the dynamical signature of this process may be subtle and largely independent of mass.

An alternative class of formation scenarios invokes circumstellar disks as the birthplace of substellar objects, perhaps through collisions of star+disk systems or intrinsic instabilities in single star+disk systems (e.g. Lin et al. 1998; Watkins et al. 1998a,b; Boss 1998). Specific predictions are lacking; e.g., for simulations of star+disk collisions, the masses of the resulting objects depend on the assumed star+disk properties and especially the orbital parameters. Nevertheless, dynamical interactions, either during the formation episode or afterwards, are needed to liberate the brown dwarfs into free-floating objects. In this respect, similarities exist with the aforementioned Reipurth & Clarke (2001) scenario. In a broader sense, all these scenarios have randomness as a central deterministic element, as opposed to, e.g., the initial conditions in pre-(sub)stellar molecular cores.

Intuition suggests that ejection will be inherently hostile to disks around young substellar objects. Studies of the encounter of a star+disk system with another passing system find that such events are highly disruptive to the disks, typically truncating the disk sizes to half the periastron distance (Clarke & Pringle 1993; Hall et al. 1996). A similar outcome is seen by Armitage & Clarke (1997) for the ejection of a star+disk system from a small stellar cluster. These effects are likely to be more severe for disks around

brown dwarfs given the shallower gravitational potential. Furthermore, such encounters are likely to trigger rapid accretion (Bonnell & Bastien 1992). Hence, Reipurth (2000) and Reipurth & Clarke (2001) predict that young brown dwarfs are unlikely to have signatures of disks, or else that such signatures will have shorter lifetimes than for young stars. This is inconsistent with our results: we find that disks around young brown dwarfs are very common. Moreover, the disks are contemporaneous with disks around the young stars in the same star-forming regions. Assuming the brown dwarfs and stars are roughly coeval, the lifetimes of brown dwarf disks are at least as long as those of stellar disks.

One possible explanation for this discrepancy could be that most of the (diskless) ejected objects have dispersed to large distances from the young stars, which would occur for ejection velocities of a few km s⁻¹. Such objects would then be missing from existing optical/IR imaging surveys. The remaining brown dwarfs would be the ones which experienced only very gentle ejections, and hence their disks would be preserved. It is not clear if such a direct correspondence between ejection velocity and disk survival can be maintained. Moreover, in such a scenario the mass function measured for IC 348 would be strongly deficient in brown dwarfs compared to the field mass function. This is not supported by the observed IMF (Luhman 1999; Najita et al. 2000).

Another possible explanation is that the post-ejection disks are truncated but they accrete at such low rates that they still retain enough disk material to produce an observable disk signature at ages of a few Myr. Detailed predictions for the effect of ejection on brown dwarf disks are not yet available, but simple estimates suggest that the surviving disks may be quite tenuous. We consider the case where the velocities of the ejected brown dwarfs are not very different than the stars, consistent with simulations of decaying few-body systems (Sterzik & Durisen 1998). For a 50 M_{Jup} object, a typical velocity of $\sim 2 \text{ km s}^{-1}$ (Jones & Herbig 1979; Hartmann et al. 1986) corresponds to the escape velocity at a distance of 10 AU. Adopting this estimate as the truncation radius, we can ask whether the disks will have enough material to persist for a few Myr. The minimum total disk mass for the presence of optically thick L'-band emission is only $\sim 10^{-7} M_{\odot}$, which would quickly be accreted for canonical accretion rates of 10^{-10} to $10^{-11} M_{\odot} \, \mathrm{yr}^{-1}$. Instead assume that the initial disk was 100 AU in size with a mass of 1% of the central object, similar to the case for T Tauri stars (Osterloh & Beckwith 1995). Assuming a surface density profile of $r^{-3/2}$ (Hayashi 1981), the truncated disk will have $(10/100)^{1/2}$ of the initial mass, or a total mass of about $10^{-4} M_{\odot}$ for a 50 M_{Jup} object. For the aforementioned accretion rates, the lifetime of these truncated disks will be about 1–10 Myr, comparable to the ages of our targets. Hence, the disk mass budget is roughly compatible with the ejection scenario. Note that this estimate is based on two assumptions: (1) the current accretion rates are roughly constant over the entire lifetime, and (2) the disk surface density profile is not perturbed significantly by the ejection+truncation event. Neither of these is likely to be

Alternatively, our finding that brown dwarf disks are

as common as disks around T Tauri stars is wellaccommodated in perhaps the simplest picture of brown dwarf formation, namely the collapse of isolated, very low mass cores — a direct analog to the conventional picture of isolated low-mass star formation. In this case, the low disk accretion rates found for young brown dwarfs may have played a more central role in their formation. That is, brown dwarfs that coexist with stars in young clusters like IC 348 may have formed like their more massive counterparts but with much lower accretion rates in order for all the objects to have accumulated their final masses on roughly the same timescale. The idea that stars of different masses result from different accretion rates is not new. For example, something similar is needed in order to explain the coexistence of high mass stars (e.g., $>20~M_{\odot}$) and low mass stars (e.g., $< 1M_{\odot}$) in young clusters (e.g. Shu et al. 1987; Myers & Fuller 1993). Since the main sequence lifetime of high mass stars is only a few Myr, they must accrete their final mass on a timescale much shorter than this in order to coexist with much lower mass stars. The mass accretion rates required ($\sim 10^{-4} M_{\odot} \text{ yr}^{-1}$) are much larger than those typically ascribed to the young progenitors of solar-mass stars. Our results suggest that a similar scenario of mass-dependent accretion rates may apply down to substellar masses.

To summarize, the widespread presence of disks around young brown dwarfs at ages of a few Myr provides prima facie evidence of a similar origin for low-mass stars and brown dwarfs. The high disk frequency is more difficult to reconcile with scenarios involving disk-disk collisions and/or premature ejection. Important future observational goals will be to determine the sizes and masses of brown dwarf disks. These cannot be measured from existing thermal-IR ($\sim 3-10~\mu m$) data, since emission at these wavelengths originates from relatively small radii ($\lesssim 1~{\rm AU}$) and is optically thick even for minute disk masses. Longer wavelength data, namely far-IR (from SIRTF) and submm (e.g., from JCMT/SCUBA and SMA) measurements are needed.

7. SUMMARY AND CONCLUDING REMARKS

We have completed the first systematic survey for circumstellar disks around young brown dwarfs and VLM stars. We have obtained L'-band imaging for objects spectroscopically classified as having very low temperatures and combined these observations with existing JHK_S data. Our sample comprises most of the published objects with spectral types from M6 to M9.5 in IC 348 and Taurus, and should be largely free of selection biases for our purposes. None appear to be binaries at a resolution of 0'.4 resolution (55–120 AU). Based on current models, our targets have masses of \sim 15 to 100 M_{Jup} and ages of \lesssim 5 Myr. Our survey is sensitive enough to detect bare substellar photospheres and hence is the first unbiased survey for disks around such low mass objects.

Using the published spectral types and extinctions, we determine the intrinsic photospheric K_S-L' (2.0–4.1 μ m) colors of our targets and hence if they have IR excesses. We find that excesses are very common, occurring in nearly 80% of the sample. Such excesses are one of the classic signatures of circumstellar disks around T Tauri stars, and there is ample observational evidence and theoretical ex-

pectation that such disks exists around young stars. Likewise, disks are the natural and most plausible explanation for the IR excesses we observe around young brown dwarfs and VLM stars. The L'-band emission arises from the inner regions of the disks, within $\lesssim 0.1$ AU, and is sensitive to disks with masses of $\gtrsim 10^{-7}~M_{\odot}$.

The observed $(K_S-L')_0$ excesses are well-correlated

The observed $(K_S-L')_0$ excesses are well-correlated with H α line emission, as in the case for T Tauri stars. This supports the idea that accretion disks are the common origin for both forms of emission. The IR excesses do not appear to correlate with any other property of the central sources. The excess frequency and amplitude are independent of the mass. However, the coolest objects in the sample, spectral type M9, have negligible excesses, indicating that their inner disk regions are empty or perhaps the objects are diskless. Given the very low estimated masses of the M9 objects ($\lesssim 15-20~M_{Jup}$), this is a tantalizing finding which should be pursued with a larger sample.

The T Tauri stars of IC 348 and Taurus exhibit comparably high disk fractions as the brown dwarfs, and therefore we find that stellar and substellar disks are contemporaneous. Assuming the populations in these regions are roughly coeval, brown dwarf disks are at least as long-lived as disks around solar-mass stars. The amplitude of the IR excesses do not show any trend with age, using the absolute K-band magnitude as a model-independent relative age scale. Most of the stellar population has an estimated age of 1–3 Myr, and assuming coevality, we infer that the inner regions of brown dwarf disks do not evolve significantly for the first \sim 3 Myr.

Given the low luminosities and weak gravitational potentials of substellar objects, one expects a priori that circumstellar disks around young brown dwarfs will be cooler and less luminous than disks around the higher mass T Tauri stars. This is confirmed by our measurements: the observed $(K_S-L')_0$ excesses are substantially smaller than those for T Tauri stars. As a consequence, a conventional analysis of the disk fraction using only IR colors would have missed most of the sources with excesses in our sample. While such analyses work well for T Tauri stars, in the case of young brown dwarfs the much reduced contrast between the disks and the photospheres is a serious impediment.

We use standard models of flat, optically thick circumstellar disks to examine the physical properties of the brown dwarf disks. The IR excesses can be explained simply by reprocessing disks — there is no need for a significant contribution from accretion luminosity. The inferred accretion rates are $\lesssim 10^{-9}~M_{\odot}~\rm yr^{-1}$, or at least an order of magnitude lower than typical for classical T Tauri stars. Nevertheless, the presence of H α emission strongly suggests that at least some accretion is ongoing. The mere existence of accreting brown dwarfs at ages of a few Myr argues for mass-dependent accretion rates, since brown dwarfs with typical T Tauri star accretion rates would not remain substellar.

The maximum observed excesses are less than those expected from a disk which extends to the stellar surface — this suggests the disks have inner holes. This inference is supported by analyzing the observed distribution of IR excesses with Monte Carlo simulations of disks viewed at random inclinations: models with hole sizes of $\approx 2R_{\star}$ are a

much better match to the observations than models without holes or those with much larger holes. The presence of an inner hole is consistent with a picture where the hole arises from the interaction of the inner disk with the magnetic field of the central object. Our rough estimates based on magnetospheric accretion models find that the brown dwarf magnetic fields are on the order of several hundred gauss, quite modest compared to measurements for T Tauri stars. The inner hole sizes for both T Tauri stars and young brown dwarfs are indicative of disk temperatures hot enough for significant thermal ionization, which is needed to permit coupling of the magnetic field to the disk. Thus, our inferred hole sizes suggest that the magnetic accretion paradigm developed for T Tauri stars may extend to substellar masses. This also illustrates one way in which brown dwarf disks may be useful laboratories for testing our understanding of the physical processes of circumstellar disks.

We have quantitatively examined the possible systematic errors and find that they are not expected to be significant. These include the uncertainties in spectral typing and extinction, disk emission contamination, surface gravity effects, sample selection bias, and the temperature scale for pre-main sequence objects. In addition, most of the plausible systematic effects, even if significant, would act to increase the disk fraction, which we already find is very high.

Our basic observational findings are that (1) most young brown dwarfs have disks, and (2) these disks are contemporaneous with disks around T Tauri stars in the same star-forming regions. The latter also demonstrates that brown dwarf disks are at least as long-lived as disks around stars, assuming that the stars and brown dwarfs are roughly coeval. These observations are naturally accommodated in a picture where brown dwarfs are born in a similar manner as stars — our results offer compelling evidence for a common origin for objects from the stellar regime down to the substellar and planetary-mass regime.

Alternative formation scenarios, such as disk-disk collisions and premature ejection, involve dynamical interactions in creating brown dwarfs. While specific predictions are lacking due to the stochastic nature of these scenarios,

brown dwarfs formed by collision and/or ejection are generally expected to have smaller and less massive disks, and consequently shorter disk lifetimes, compared to brown dwarfs formed in isolation. This expectation conflicts with our finding that brown dwarf disks are at least as long-lived as disks around young stars.

We have found that brown dwarf disks are common. In order to better understand the nature of these disks, longer wavelength (far-IR, sub-mm, and mm) measurements are needed to determine the disk masses and sizes. More measurements of the accretion rates are sorely needed. The lifetimes of disks around brown dwarfs and the disk frequency at even lower masses ($\lesssim 15~M_{Jup}$) are also outstanding questions. These studies will be important for determining the origin of brown dwarfs and their disks, and also for placing these objects in context with our physical understanding of the star formation process. Finally, the very high disk fraction of young brown dwarfs raises the possibility of forming planets around brown dwarfs. Such planetary systems would represent a fascinating alternative to the numerous planetary systems found around solar-type stars.

It is a pleasure to thank Charlie Lada, James Muzerolle, John Tonry, and Jonathan Williams for useful discussions. We are grateful to support from the staff of UKIRT observatory, especially Thor Wold and Paul Hirst, which made these observations possible. We thank Sandy Leggett for updated information on the standard stars and for making filter curves and her published photometry readily available. We thank Kevin Luhman for providing unpublished $H\alpha$ measurements. UKIRT is operated by the Joint Astronomy Centre on behalf of the U.K. Particle Physics and Astronomy Research Council. This research has made use of data products from the Two Micron All Sky Survey, which is a joint project of the University of Massachusetts and the Infrared Processing and Analysis Center/California Institute of Technology, funded by NASA and NSF. This research has also made use of NASA's Astrophysics Data System Abstract Service. M. Liu is grateful for research support from the Beatrice Watson Parrent Fellowship at the University of Hawai'i.

APPENDIX

CALCULATING THE DISK FRACTION IN THE PRESENCE OF OBSERVATIONAL ERRORS

In the literature, the usual means of computing the disk fraction assumes only Poisson counting statistics contribute to the uncertainty in the result. Consider a sample of N objects, each with a color excess Δ_i , which can be derived from a single color (as in the case of our work here) or many colors (e.g., a color-color diagram). Typically, one then defines the number of sources with disks as

$$N_{disk} = \sum_{i} (\Delta_i > \Delta_0) \tag{A1}$$

where the notation represents the number of measurements greater than a specified constant Δ_0 . Many studies choose $\Delta_0 = 0$, i.e., any color excess is taken as the sign of a disk (e.g. Lada & Lada 1995; Haisch et al. 2001a). The disk fraction and its error are then

$$f_{disk} = \frac{N_{disk}}{N} \tag{A2}$$

$$\sigma(f_{disk}) = \frac{\sqrt{N_{disk}}}{N} , \qquad (A3)$$

respectively. Clearly, this approach neglects the effects of measurement errors: a sample with very large errors in the Δ_i 's should lead to a larger $\sigma(f_{disk})$ than a sample with small errors. Only in the case of zero measurement errors will $\sigma(f_{disk})$

be given exactly by equation (A3). Hence, the published disk fraction errors are somewhat underestimated. Some studies attempt to circumvent the influence of observational errors by setting $\Delta_0 > 0$, typically choosing a value comparable to the measurement errors (e.g. Strom et al. 1989; Hillenbrand et al. 1998). However, this approach inevitably excludes some objects with genuine disk excesses, and hence the disk fractions are somewhat underestimated.

We use a simple Monte Carlo approach to account for both Poisson counting errors and measurement errors in determining the disk fraction.⁶ Our observed sample is composed of N objects, each with a color index Δ_i and measurement error ϵ_i . For each Monte Carlo realization, we generate a set of N objects having color indices

$$\Delta_i' = \Delta_i + (\mathcal{G}_i \times \epsilon_i) \tag{A4}$$

where \mathcal{G}_i is drawn from a normal distribution of zero mean and unit variance. We then determine the number of sources with $\Delta_i'>0$, denoted as \overline{N}_{disk}^j . (The subscript i denotes different objects, and the superscript j denotes different Monte Carlo realizations.) For each realization, we assume the resulting number of sources with disks is subject to counting statistics: namely, the number of disk sources is described by a Poisson distribution of mean \overline{N}_{disk}^j , which we denote as $\mathcal{P}(N_{disk}^j; \overline{N}_{disk}^j)$. After a large number of realizations (we use 100,000), we sum all the individual Poisson distributions to form a probability distribution function for the number of disk sources:

$$PDF(N_{disk}) = \sum_{j} \mathcal{P}(N_{disk}^{j}; \overline{N}_{disk}^{j}) .$$
 (A5)

Second Incremental Data Release

We then compute the disk fraction using the value of N_{disk} at the peak of the PDF and use the standard deviation of the PDF (well approximated by fitting a gaussian) as the error in N_{disk} .

The net result of using this Monte Carlo approach is that our tabulated disk fractions are $\approx 5\%$ smaller than simply using the standard approach (i.e., equation (A1) with $\Delta_0 = 0$) and the errors in the disk fraction are $\approx 5\%$ larger. The effects are small because of the relatively high S/N of the $(K_S - L')_0$ excess measurements (median error of 0.09 mag). Note that these percentages should not be used as a general representation for all disk fraction calculations. The result of ignoring the measurement errors in Δ_i will depend on a particular sample's properties, namely the size of the sample, the distribution of excesses, and the measurement errors.

REFERENCES

Adams, F. C., Lada, C. J., & Shu, F. H. 1987, ApJ, 312, 788
Adams, F. C. & Shu, F. H. 1986, ApJ, 308, 836
Apai, D., Pascucci, I., Henning, T., Sterzik, M. F., Klein, R., Semenov, D., Günther, E., & Stecklum, B. 2002, ApJ, 573, L115
Armitage, P. J. & Bonnell, I. A. 2002, MNRAS, 330, L11
Armitage, P. J. & Clarke, C. J. 1997, MNRAS, 285, 540 Baraffe, I., Chabrier, G., Allard, F., & Hauschildt, P. H. 1998, A&A, 2002, A&A, 382, 563 Barrado y Navascués, D., Zapatero Osorio, M. R., Béjar, V. J. S., Rebolo, R., Martín, E. L., Mundt, R., & Bailer-Jones, C. A. L. 2001, A&A, 377, L9 Basri, G. 1998, in ASP Conf. Ser. 134: Brown Dwarfs and Extrasolar Bate, M. R., Bonnell, I. A., & Bromm, V. 2002, MNRAS, 332, L65 Bertout, C., Basri, G., & Bouvier, J. 1988, ApJ, 330, 350 Bessell, M. S. & Brett, J. M. 1988, PASP, 100, 1134 Bonnell, I. & Bastien, P. 1992, ApJ, 401, L31 Bontemps, S. et al. 2001, A&A, 372, 173
Boss, A. P. 1998, ApJ, 503, 923
Bouvier, J., Stauffer, J. R., Martin, E. L., Barrado y Navascues, D.,
Wallace, B., & Bejar, V. J. S. 1998, A&A, 336, 490 Briceño, C., Hartmann, L., Stauffer, J., & Martin, E. 1998, AJ, 115, Burgasser, A. J. et al. 2002, ApJ, 564, 421 Burrows, A., Marley, M., Hubbard, W. B., Lunine, J. I., Guillot, T., Saumon, D., Freedman, R., Sudarsky, D., & Sharp, C. 1997, ApJ, Burrows, C. J. et al. 1996, ApJ, 473, 437 Calvet, N. & Gullbring, E. 1998, ApJ, 509, 802 Calvet, N., Magris, G. C., Patino, A., & D'Alessio, P. 1992, Revista Mexicana de Astronomia y Astrofisica, 24, 27 Campbell, B., Walker, G. A. H., & Yang, S. 1988, ApJ, 331, 902 Carpenter, J. M. 2001, AJ, 121, 2851 Clarke, C. J. & Pringle, J. E. 1993, MNRAS, 261, 190 Comerón, F., Neuhaüser, R., & Kaas, A. A. 2000, A&A, 359, 269 Comerón, F., Rieke, G. H., Claes, P., Torra, J., & Laureijs, R. J.

Cuby, J. G., Saracco, P., Moorwood, A. F. M., D'Odorico, S.,
 Lidman, C., Comerón, F., & Spyromilio, J. 1999, A&A, 349, L41
 Cushing, M. C., Tokunaga, A. T., & Kobayashi, N. 2000, AJ, 119,

1998, A&A, 335, 522

D'Antona, F. & Mazzitelli, I. 1997, Memorie della Societa Astronomica Italiana, 68, 807
Delfosse, X. et al. 1999, A&AS, 135, 41
Edwards, S. 1995, in Revista Mexicana de Astronomia y Astrofisica Conference Series, Vol. 1, 309
Elias, J. H. 1978, ApJ, 224, 857
Els, S. G., Sterzik, M. F., Marchis, F., Pantin, E., Endl, M., & Kürster, M. 2001, A&A, 370, L1
Fromang, S., Terquem, C., & Balbus, S. A. 2002, MNRAS, 329, 18
Gizis, J. E., Monet, D. G., Reid, I. N., Kirkpatrick, J. D., Liebert, J., & Williams, R. J. 2000, AJ, 120, 1085
Guenther, E. W., Lehmann, H., Emerson, J. P., & Staude, J. 1999, A&A, 341, 768
Gullbring, E., Hartmann, L., Briceno, C., & Calvet, N. 1998, ApJ, 492, 323
Haisch, K. E., Lada, E. A., & Lada, C. J. 2001a, AJ, 121, 2065
—. 2001b, ApJ, 553, L153
Haisch, K. E., Lada, E. A., Piña, R. K., Telesco, C. M., & Lada, C. J. 2001c, AJ, 121, 1512
Halbwachs, J. L., Arenou, F., Mayor, M., Udry, S., & Queloz, D. 2000, A&A, 355, 581
Hall, S. M., Clarke, C. J., & Pringle, J. E. 1996, MNRAS, 278, 303
Hartigan, P., Edwards, S., & Ghandour, L. 1995, ApJ, 452, 736
Hartigan, P., Hartmann, L., Kenyon, S. J., Strom, S. E., & Skrutskie, M. F. 1990, ApJ, 354, L25
Hartmann, L., Hewett, R., & Calvet, N. 1994, ApJ, 426, 669
Hartmann, L., Hewett, R., & Calvet, N. 1994, ApJ, 426, 669
Hartmann, L., Hewett, R., & Calvet, N. 1994, ApJ, 426, 669
Hartmann, L., Hewett, R., Stahler, S., & Mathieu, R. D. 1986, ApJ, 309, 275
Hawarden, T. G., Leggett, S. K., Letawsky, M. B., Ballantyne, D. R., & Casali, M. M. 2001, MNRAS, 325, 563
Hawley, S. L. et al. 2002, AJ, in press (astro-ph/0204065)
Hayashi, C. 1981, Progress of Theoretical Physics Supplement, 70, 35
Herbig, G. H. 1998, ApJ, 497, 736
Hillenbrand, L. A. 1997, AJ, 113, 1733
Hillenbrand, L. A. & Carpenter, J. M. 2000, ApJ, 540, 236

Cutri, R. M. et al. 2000, Explanatory Supplement to the 2MASS

⁶ Kenyon & Gómez (2001) use a Monte Carlo approach to account for measurement errors and uncertainty in the extinction law when computing the disk fraction. However, they neglect Poisson errors in their computations.

Hillenbrand, L. A., Strom, S. E., Calvet, N., Merrill, K. M., Gatley, I., Makidon, R. B., Meyer, M. R., & Skrutskie, M. F. 1998, AJ, 116, 1816 Imanishi, K., Koyama, K., & Tsuboi, Y. 2001, ApJ, 557, 747 Joergens, V. & Guenther, E. 2001, A&A, 379, L9 Johns-Krull, C. M. & Valenti, J. A. 1996, ApJ, 459, L95 Johns-Krull, C. M., Valenti, J. A., Hatzes, A. P., & Kanaan, A. 1999a, ApJ, 510, L41

Jones, B. F. & Herbig, G. H. 1979, AJ, 84, 1872 Kenyon, S. J., Dobrzycka, D., & Hartmann, L. 1994, AJ, 108, 1872 Kenyon, S. J. & Gómez, M. 2001, AJ, 121, 2673

Johns-Krull, C. M., Valenti, J. A., & Koresko, C. 1999b, ApJ, 516,

Kenyon, S. J. & Hartmann, L. 1987, ApJ, 323, 714

-. 1995, ApJS, 101, 117

—. 1995, ApJS, 101, 117

Kenyon, S. J. & Hartmann, L. W. 1990, ApJ, 349, 197

Kenyon, S. J., Yi, I., & Hartmann, L. 1996, ApJ, 462, 439

Kirkpatrick, J. D., Reid, I. N., Liebert, J., Cutri, R. M., Nelson, B., Beichman, C. A., Dahn, C. C., Monet, D. G., Gizis, J. E., & Skrutskie, M. F. 1999, ApJ, 519, 802

Königl, A. 1991, ApJ, 370, L39

Lada, C. J. & Adams, F. C. 1992, ApJ, 393, 278

Lada, E. A. & Lada, C. J. 1995, AJ, 109, 1682

Leggett, S. K. 1992, ApJS, 82, 351

Leggett, S. K., Allard, F., Dahn, C., Hauschildt, P. H., Kerr, T. H., & Rayner, J. 2000, ApJ, 535, 965

Leggett, S. K., Allard, F., Geballe, T. R., Hauschildt, P. H., & Schweitzer, A. 2001, ApJ, 548, 908

Leggett, S. K., Allard, F., & Hauschildt, P. H. 1998, ApJ, 509, 836

Leggett, S. K. et al. 2002, ApJ, 564, 452

Lin, D. N. C., Laughlin, G., Bodenheimer, P., & Rozyczka, M. 1998, Science, 281, 2025

Science, 281, 2025 Liu, M. C. 2001, in Twelfth Cambridge Workshop on Cool Stars,

Stellar Systems, and the Sun, ASP. Conf. Series, in press Liu, M. C., Fischer, D. A., Graham, J. R., Lloyd, J. P., Marcy, G. W., & Butler, R. P. 2001, ApJ, in press (astro-ph/0112407)

Liu, M. C., Wainscoat, R., Martín, E. L., Barris, B., & Tonry, J.

2002, ApJ, 568, L107 Lucas, P. W., Roche, P. F., Allard, F., & Hauschildt, P. H. 2001, MNRAS, 326, 695

Luhman, K. L. 1999, ApJ, 525, 466

2000, ApJ, 544, 1044

Luhman, K. L., Briceno, C., Rieke, G. H., & Hartmann, L. 1998a, ApJ, 493, 909

Luhman, K. L., Liebert, J., & Rieke, G. H. 1997, ApJ, 489, L165 Luhman, K. L., Rieke, G. H., Lada, C. J., & Lada, E. A. 1998b, ApJ, 508, 347

Luhman, K. L., Rieke, G. H., Young, E. T., Cotera, A. S., Chen, H., Rieke, M. J., Schneider, G., & Thompson, R. I. 2000, ApJ, 540,

Lynden-Bell, D. & Pringle, J. E. 1974, MNRAS, 168, 603 Marcy, G. W. & Benitz, K. J. 1989, ApJ, 344, 441

Marcy, G. W. & Butler, R. P. 1998, ARA&A, 36, 57
Marcy, G. W., Butler, R. P., Vogt, S. S., Liu, M. C., Laughlin, G., Apps, K., Graham, J. R., Lloyd, J., Luhman, K. L., & Jayawardhana, R. 2001, ApJ, 555, 418

Martín, E. L., Dougados, C., Magnier, E., Ménard, F., Magazzù, A., Cuillandre, J.-C., & Delfosse, X. 2001, ApJ, 561, L195 Mathis, J. 2000, in Allen's Astrophysical Quantities, 4th edn., ed.

A. N. Cox (New York: AIP Press), 527

Meyer, M. R., Calvet, N., & Hillenbrand, L. A. 1997, AJ, 114, 288 Moraux, E., Bouvier, J., & Stauffer, J. R. 2001, A&A, 367, 211 Muench, A. A., Alves, J., Lada, C. J., & Lada, E. A. 2001, ApJ, 558,

Muzerolle, J., Briceño, C., Calvet, N., Hartmann, L., Hillenbrand, L., & Gullbring, E. 2000, ApJ, 545, L141

Muzerolle, J. et al. 2002, in IAU 211: Brown Dwarfs, ed. E. Martín, ASP. Conf. Series, in press

Myers, P. C. & Fuller, G. A. 1993, ApJ, 402, 635

Myers, P. C., Fuller, G. A., Mathieu, R. D., Beichman, C. A., Benson,

P. J., Schild, R. E., & Emerson, J. P. 1987, ApJ, 319, 340 Najita, J. R., Tiede, G. P., & Carr, J. S. 2000, ApJ, 541, 977 Natta, A. & Testi, L. 2001, A&A, 376, L22

Natta, A., Testi, L., Comerón, F., Oliva, E., D'Antona, F., Baffa, C., Comoretto, G., & Gennari, S. 2002, A&A, 393, 597

Oliveira, J. M., Jeffries, R. D., Kenyon, M. J., Thompson, S. A., & Naylor, T. 2002, A&A, 382, L22
Osterloh, M. & Beckwith, S. V. W. 1995, ApJ, 439, 288
Ostriker, E. C. & Shu, F. H. 1995, ApJ, 447, 813
Palla, F. & Stahler, S. W. 2000, ApJ, 540, 255

Pickett, B. K., Durisen, R. H., Cassen, P., & Mejia, A. C. 2000, ApJ, 540, L95

Pollack, J. B., Hubickyj, O., Bodenheimer, P., Lissauer, J. J., Podolak, M., & Greenzweig, Y. 1996, Icarus, 124, 62

Potter, D., Martín, E. L., Cushing, M. C., Baudoz, P., Brandner, W., Guyon, O., & Neuhäuser, R. 2002, ApJ, 567, L133 Pourbaix, D. & Arenou, F. 2001, A&A, 372, 935

Preibisch, T. & Zinnecker, H. 2001, AJ, 122, 866

—. 2002, AJ, 123, 1613 Press, W. H., Teukolsky, S. A., Vetterling, W. T., & Flannery, B. P. 1992, Numerical Recipes in C: The Art of Scientific Computing (Cambridge: Cambridge University Press, 2nd ed.)

Reipurth, B. 2000, AJ, 120, 3177 Reipurth, B. & Clarke, C. 2001, AJ, 122, 432

Reipurth, B., Clarke, C., & Delgado-Donate, E. 2001, in Twelfth Cambridge Workshop on Cool Stars, Stellar Systems, and the Sun: The Future of Cool-Star Astrophysics, in press (astro-ph/0110481) Shu, F., Najita, J., Galli, D., Östriker, E., & Lizano, S. 1993, in Protostars and Planets III, 3

Shu, F., Najita, J., Ostriker, E., Wilkin, F., Ruden, S., & Lizano, S. 1994, ApJ, 429, 781

Shu, F. H., Adams, F. C., & Lizano, S. 1987, ARA&A, 25, 23 Simons, D. A. & Tokunaga, A. T. 2001, PASP, in press (astroph/0110594)

Skrutskie, M. F., Dutkevitch, D., Strom, S. E., Edwards, S., Strom,

Skrutskie, M. F., Dutkevitch, D., Strom, S. E., Edwards, S., Strom, K. M., & Shure, M. A. 1990, AJ, 99, 1187
Stauffer, J. R., Schild, R., Barrado y Navascues, D., Backman, D. E., Angelova, A. M., Kirkpatrick, J. D., Hambly, N., & Vanzi, L. 1998, ApJ, 504, 805
Sterzik, M. F. & Durisen, R. H. 1998, A&A, 339, 95
Strom, K. M., Strom, S. E., Edwards, S., Cabrit, S., & Skrutskie, M. F. 1989, AJ, 97, 1451
Testi, L., Natta, A., Oliva, E., D'Antona, F., Comeron, F., Baffa, C., Comoretto, G., & Gennari, S. 2002, ApJ, 571, L155

 1esu, L., Natta, A., Oliva, E., D'Antona, F., Comeron, F., Baffa, C., Comoretto, G., & Gennari, S. 2002, ApJ, 571, L155
 Tokunaga, A. T., Simons, D. A., & Vacca, W. D. 2001, PASP, in press (astro-ph/0110593)
 Tsuji, T., Ohnaka, K., & Aoki, W. 1996, A&A, 305, L1
 Udry, S., Mayor, M., Naef, D., Pepe, F., Queloz, D., Santos, N. C., & Burnet, M. 2002, A&A, submitted (astro-ph/0202458)
 Umebayashi, T. & Nakapa, T. 1988, Prog. Theo. Phys. Supp. 26 Umebayashi, T. & Nakano, T. 1988, Prog. Theo. Phys. Supp., 96,

Valenti, J. A., Basri, G., & Johns, C. M. 1993, AJ, 106, 2024 Walker, G. A. H., Walker, A. R., Irwin, A. W., Larson, A. M., Yang, S. L. S., & Richardson, D. C. 1995, Icarus, 116, 359
Watkins, S. J., Bhattal, A. S., Boffin, H. M. J., Francis, N., & Whitworth, A. P. 1998a, MNRAS, 300, 1205

1998b, MNRAS, 300, 1214

Wilking, B. A., Greene, T. P., & Meyer, M. R. 1999, AJ, 117, 469 Wood, K., Lada, C. J., Bjorkman, J. E., Kenyon, S. J., Whitney, B., & Wolff, M. J. 2002, ApJ, 567, 1183

Zapatero Osorio, M. R., Béjar, V. J. S., Martin, E. L., Barrado y Navascués, D., & Rebolo, R. 2002a, ApJ, 569, L99 Zapatero Osorio, M. R., Béjar, V. J. S., Pavlenko, Y., Rebolo, R.,

Allende Prieto, C., Martín, E. L., & García López, R. J. 2002b, A&A, 384, 937

Zapatero Osorio, M. R., Bejar, V. J. S., Martin, E. L., Rebolo, R., Barrado Y Navascues, D., Bailer-Jones, C. A. L., & Mundt, R. 2000, Science, 290, 103 Zucker, S. & Mazeh, T. 2001, ApJ, in press (astro-ph/0107124)

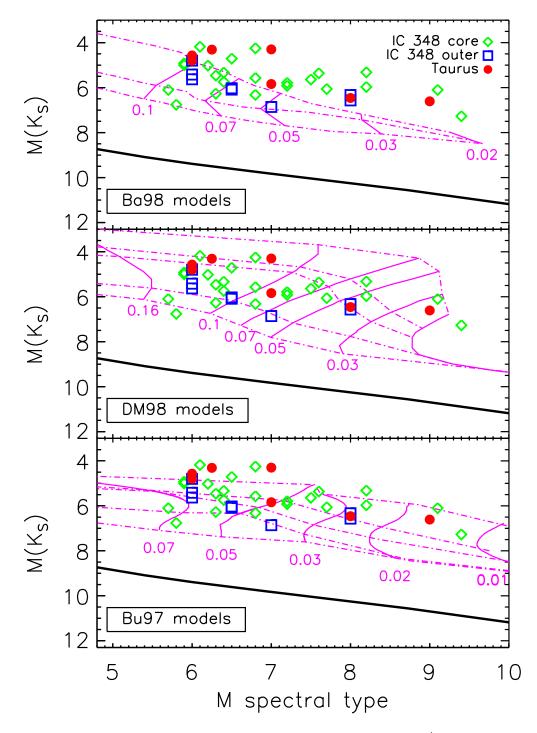


Fig. 1.— Dereddened absolute K_S -band magnitude and spectral type for our L'-band sample. Magnitude errors are comparable to the symbol size, and spectral type errors are $\lesssim 0.5$ subclasses. The main-sequence is shown as a heavy line. Dotted lines are model isochrones while solid lines show models of constant mass in units of M_{\odot} . The Luhman (1999) temperature scale is used to convert the model temperatures to spectral type. **Top:** Baraffe et al. (1998, 2002) models. The isochrones are for ages of 1, 5, and 10 Myr. **Middle:** D'Antona & Mazzitelli (1997) models. The isochrones are for ages of 0.1, 0.5, 1.0, 5.0, and 10.0 Myr. **Bottom:** Burrows et al. (1997) models. The isochrones are for ages of 0.1, 0.5, 1.0, 5.0, and 10.0 Myr.

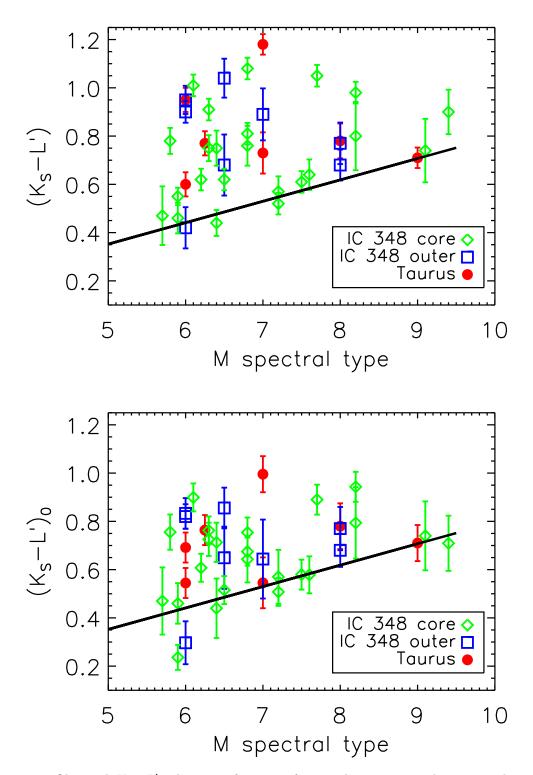


Fig. 2.— **Top:** Observed $K_S - L'$ colors as a function of spectral type. Typical errors in the spectral type are 0.5 subclasses or less. The heavy line represents the colors of field M dwarfs (see § 2.3 for references). **Bottom:** Dereddened $K_S - L'$ colors. Most of the objects show IR emission in excess of that expected from their photospheres.

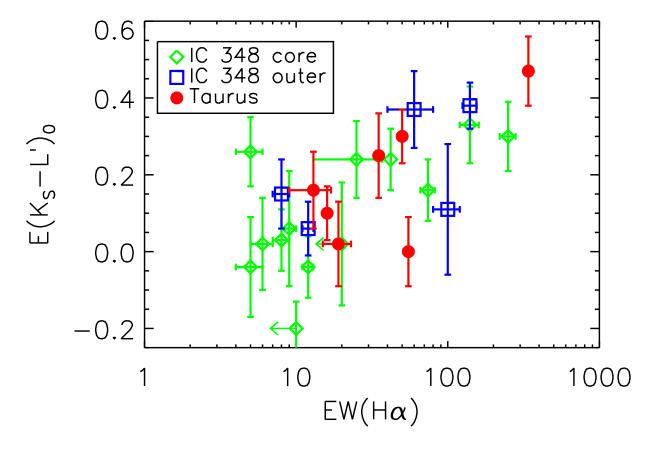


Fig. 3.— Relation between intrinsic IR excess and equivalent width of $H\alpha$ emission in Angstroms for the 23 objects where such data are available along with $H\alpha$ upper limits for 2 objects. The two quantities are correlated at the 3σ level, based on a Spearman rank correlation test. This supports the idea that the optical and near-IR emission both originate from the same phenomenon, namely circumstellar accretion disks.

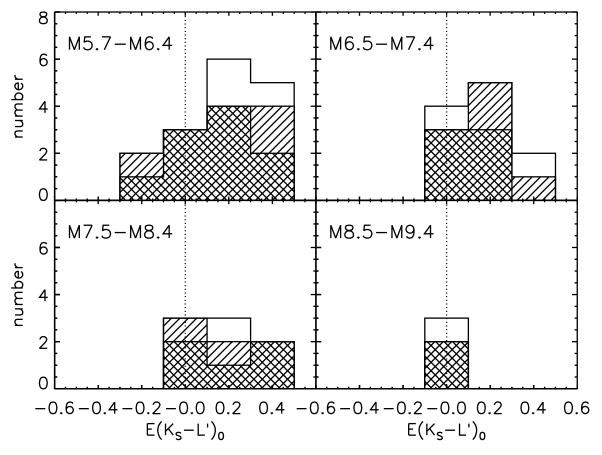


Fig. 4.— Histogram of $(K_S-L')_0$ excesses as a function of spectral type. The median $\pm 1\sigma$ measurement errors $(\pm 0.09 \text{ mag})$ are comparable to the bin width. The clear bins represent the Taurus sample; the single-hatched bins represent the outer IC 348 sample (Luhman 1999); and the double-hatched bins represent the IC 348 core sample (Najita et al. 2000). The distribution of excesses among the three earliest spectral type bins (M5.7–M6.4, M6.5–M7.4, and M7.5–8.4) are consistent with being drawn from the same parent population based on the K-S test. Hence, there is no strong evidence for the IR excesses being dependent on the mass of the central object.

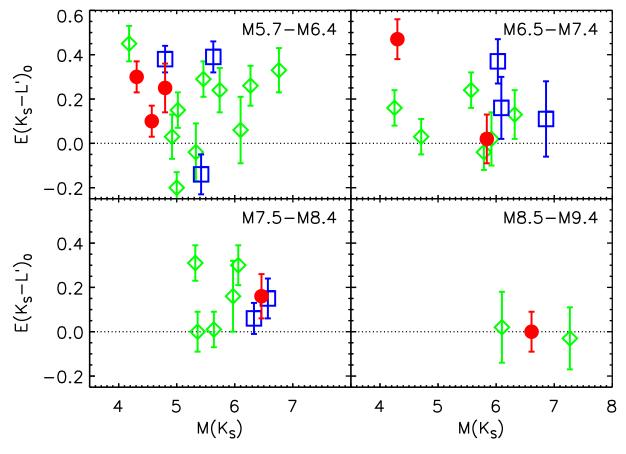


Fig. 5.— IR excess as a function of dereddened absolute K_S -band magnitude. At fixed spectral type, M_{K_S} is a proxy for the relative age, since the evolutionary tracks for young objects are approximately constant in temperature for a given mass. No statistically significant correlation with M_{K_S} exists for each spectral type bin, suggesting the inner disk regions do not evolve substantially over the first ~ 3 Myr. The symbols represent the different sub-samples and have the same meanings as in Figure 1. Errors in M_{K_S} are ≈ 0.2 mag, about twice the size of the plotting symbols.

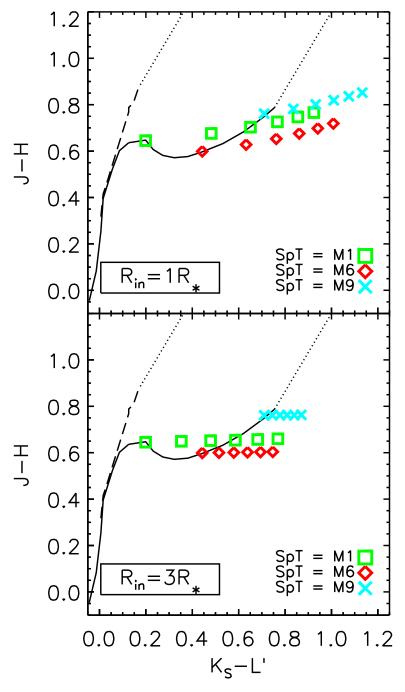


Fig. 6.— Flat blackbody reprocessing disk models plotted on JHK_SL' color-color diagrams. The locus of main sequence stars is shown as a solid line and that of giant stars as a dashed line. (See § 4.1 for details.) The two dotted lines represent the reddening vector, and the area in between is the locus of reddened stars. Each plot shows models with different inner disk radii, and the symbols indicate the spectral type of the central star. The symbols are equally spaced in $\cos \theta$ from 0 to 1, where θ is the viewing angle.

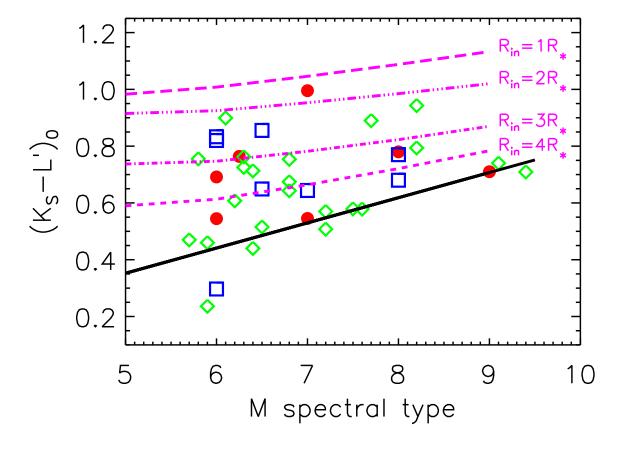


Fig. 7.— Dereddened K_S-L' colors for our targets (same data and symbols as in Figure 2) compared with face-on reprocessing disk models. Disk models with different inner hole radii are labeled in units of the stellar radius, i.e., $R_{in}=1R_{\star}$ means there is no hole. The maximum observed IR excesses are less those expected from a disk with no inner hole, and suggests $R_{in} \gtrsim 2R_{\star}$ is the more likely situation. Notice also that the observed small/non-existent $(K_S-L')_0$ excesses of the coolest objects, which are spectral type M9, suggest either disks with very large inner holes or no disks at all.

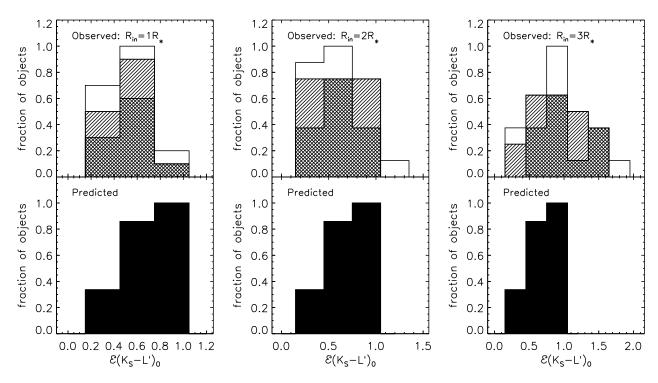


Fig. 8.— Comparison of the observed IR excess distribution with passive disk models possessing different inner radii. Disk models with inner radii (R_{in}) of 1, 2, and $3R_{\star}$ are shown. For a given disk model, the observed $(K_S-L')_0$ excess is divided by the maximum possible model excess (i.e., a face-on disk) to form the normalized color excess $\mathcal{E}(K_S-L')_0$, which is independent of the central object's temperature. The top panels show the observations. Different shadings indicate different sub-samples: Taurus (clear bins), IC 348 outer sample (single-hatched bins), and IC 348 core sample (double-hatched bins). The bottom panels plot the normalized color excess distribution for a set of disk models seen from randomly chosen viewing angles. The observations agree best with the $R_{in} = 2R_{\star}$ models, suggesting that disks around young brown dwarfs have inner holes. See § 4.2 for details.

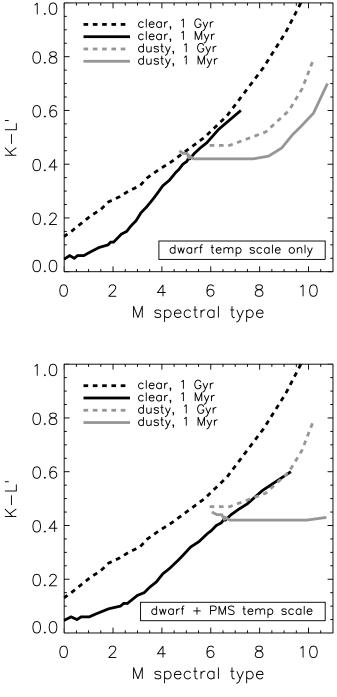


Fig. 9.— The effect of surface gravity on K-L' colors, based on models by Baraffe et al. (1998, 2002). Dust-free ("clear") models are plotted in black, and dusty models in grey. Models with ages of 1 Gyr (higher surface gravity) are converted to spectral types using a dwarf temperature scale. Models with ages of 1 Myr (lower surface gravity) use either the dwarf temperature scale (*upper plot*) or the Luhman (1999) pre-main sequence scale (*lower plot*). For our objects' spectral types, the lower surface gravity of young objects is predicted to lead to ≈ 0.1 mag bluer colors; the observations suggest the effect is even smaller. See § 5.3 for details.

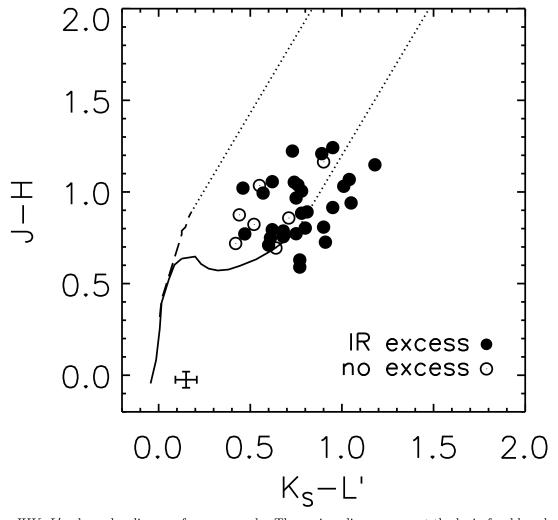


Fig. 10.— JHK_SL' color-color diagram for our sample. The various lines represent the loci of reddened giant and dwarf stars (see Figure 6 caption). Median errors are plotted in the lower right. Based on a conventional color-color analysis, one would identify only 11 out of 36 objects (those to the right of the dotted reddening band) as having IR excesses. However, our analysis incorporating the objects' spectral types shows that in fact many more (31 out of 36) have IR excesses: these are plotted as filled circles (\bullet). The majority of sources with disks are missed in the color-color diagram because their IR excesses are modest. A similar analysis using only JHK_S colors would miss nearly all the objects with IR excesses.

Table 1
Infrared Photometry

$\begin{array}{c ccccccccccccccccccccccccccccccccccc$	Object	Spectral Type	$A_K \text{ (mag)}$	L' (mag)	$E(K_S-L')_0$ (mag)					
$\begin{array}{c ccccccccccccccccccccccccccccccccccc$	IC 348: core sample									
$\begin{array}{c ccccccccccccccccccccccccccccccccccc$	NTC 075-07	$M5.7 \pm 0.6$	0.00 ± 0.11	13.03 ± 0.12	0.06 ± 0.15					
$\begin{array}{c ccccccccccccccccccccccccccccccccccc$										
$\begin{array}{c ccccccccccccccccccccccccccccccccccc$			0.00 ± 0.09							
$\begin{array}{c} {\rm NTC~044-04} & {\rm M6.2\pm0.6} & {\rm 0.02\pm0.06} & {\rm 11.82\pm0.04} & {\rm 0.15\pm0.08} \\ {\rm NTC~055-02} & {\rm M6.3\pm0.6} & {\rm 0.24\pm0.06} & {\rm 12.19\pm0.04} & {\rm 0.29\pm0.08} \\ {\rm NTC~014-05} & {\rm M6.3\pm0.6} & {\rm 0.04\pm0.07} & {\rm 12.96\pm0.05} & {\rm 0.26\pm0.09} \\ {\rm NTC~011-02} & {\rm M6.4\pm0.6} & {\rm 0.00\pm0.08} & {\rm 12.42\pm0.05} & {\rm -0.04\pm0.13} \\ {\rm NTC~075-06} & {\rm M6.4\pm0.7} & {\rm 0.06\pm0.06} & {\rm 12.45\pm0.07} & {\rm 0.24\pm0.10} \\ {\rm NTC~051-01} & {\rm M6.5\pm0.6} & {\rm 0.17\pm0.06} & {\rm 11.66\pm0.04} & {\rm 0.03\pm0.08} \\ {\rm NTC~062-01} & {\rm M6.8\pm0.7} & {\rm 0.19\pm0.08} & {\rm 13.15\pm0.08} & {\rm 0.13\pm0.11} \\ {\rm NTC~014-04} & {\rm M6.8\pm0.6} & {\rm 0.22\pm0.06} & {\rm 11.06\pm0.04} & {\rm 0.16\pm0.08} \\ {\rm NTC~022-05} & {\rm M6.8\pm0.6} & {\rm 0.53\pm0.07} & {\rm 12.42\pm0.04} & {\rm 0.24\pm0.08} \\ {\rm NTC~045-02} & {\rm M7.1\pm0.6} & {\rm 0.00\pm0.10} & {\rm 12.59\pm0.04} & {\rm -0.31\pm0.09^a} \\ {\rm NTC~045-02} & {\rm M7.1\pm0.6} & {\rm 0.00\pm0.10} & {\rm 12.59\pm0.04} & {\rm -0.31\pm0.09^a} \\ {\rm NTC~011-01} & {\rm M7.2\pm0.6} & {\rm 0.00\pm0.15} & {\rm 12.75\pm0.06} & {\rm 0.02\pm0.12} \\ {\rm NTC~013-05} & {\rm M7.5\pm0.6} & {\rm 0.05\pm0.07} & {\rm 12.48\pm0.04} & {\rm 0.01\pm0.08} \\ {\rm NTC~013-05} & {\rm M7.5\pm0.6} & {\rm 0.05\pm0.07} & {\rm 12.48\pm0.04} & {\rm 0.01\pm0.08} \\ {\rm NTC~043-03} & {\rm M7.6\pm0.6} & {\rm 0.05\pm0.07} & {\rm 12.48\pm0.04} & {\rm 0.01\pm0.08} \\ {\rm NTC~043-06} & {\rm M8.2\pm0.6} & {\rm 0.05\pm0.07} & {\rm 12.48\pm0.04} & {\rm 0.01\pm0.08} \\ {\rm NTC~043-06} & {\rm M7.7\pm0.7} & {\rm 0.26\pm0.07} & {\rm 12.67\pm0.04} & {\rm 0.30\pm0.09} \\ {\rm NTC~013-06} & {\rm M7.7\pm0.7} & {\rm 0.26\pm0.07} & {\rm 12.68\pm0.04} & {\rm 0.00\pm0.09} \\ {\rm NTC~013-06} & {\rm M7.7\pm0.7} & {\rm 0.00\pm0.09} & {\rm 12.67\pm0.04} & {\rm 0.30\pm0.09} \\ {\rm NTC~015-06} & {\rm M9.1\pm0.7} & {\rm 0.00\pm0.09} & {\rm 12.69\pm0.03} & {\rm -0.14\pm0.09} \\ {\rm NTC~015-06} & {\rm M9.1\pm0.7} & {\rm 0.00\pm0.09} & {\rm 12.69\pm0.03} & {\rm -0.14\pm0.09} \\ {\rm L99~312} & {\rm M6.0\pm0.2} & {\rm 0.13\pm0.04} & {\rm 12.27\pm0.05} & {\rm 0.39\pm0.07} \\ {\rm L99~363} & {\rm M6.5\pm0.5} & {\rm 0.50\pm0.04} & {\rm 12.69\pm0.08} & {\rm -0.14\pm0.09} \\ {\rm M9.4\pm0.9} & {\rm 0.31\pm0.04} & {\rm 12.20\pm0.06} & {\rm 0.00\pm0.04} & {\rm 0.10\pm0.07} \\ {\rm L99~363} & {\rm M8.0\pm0.2} & {\rm 0.00\pm0.04} & {\rm 13.05\pm0.05} & {\rm 0.06\pm0.07} \\ {\rm L99~363} & $										
$\begin{array}{c} {\rm NTC~055\text{-}02} & {\rm M6.3\pm0.6} & 0.24\pm0.06 & 12.19\pm0.04 & 0.29\pm0.08 \\ {\rm NTC~014\text{-}05} & {\rm M6.3\pm0.6} & 0.04\pm0.07 & 12.96\pm0.05 & -0.26\pm0.09 \\ {\rm NTC~011\text{-}02} & {\rm M6.4\pm0.6} & 0.00\pm0.18 & 12.29\pm0.05 & -0.04\pm0.13 \\ {\rm NTC~075\text{-}06} & {\rm M6.4\pm0.7} & 0.06\pm0.06 & 12.45\pm0.07 & 0.24\pm0.10 \\ {\rm NTC~051\text{-}01} & {\rm M6.5\pm0.6} & 0.17\pm0.06 & 11.66\pm0.04 & 0.03\pm0.08 \\ {\rm NTC~062\text{-}01} & {\rm M6.8\pm0.7} & 0.19\pm0.08 & 13.15\pm0.08 & 0.13\pm0.11 \\ {\rm NTC~014\text{-}04} & {\rm M6.8\pm0.6} & 0.22\pm0.06 & 11.06\pm0.04 & 0.16\pm0.08 \\ {\rm NTC~014\text{-}04} & {\rm M6.8\pm0.6} & 0.22\pm0.06 & 11.06\pm0.04 & 0.16\pm0.08 \\ {\rm NTC~045\text{-}02} & {\rm M7.1\pm0.6} & 0.00\pm0.10 & 12.59\pm0.04 & -0.31\pm0.09^a \\ {\rm NTC~045\text{-}02} & {\rm M7.1\pm0.6} & 0.00\pm0.15 & 12.75\pm0.06 & 0.02\pm0.12 \\ {\rm NTC~011\text{-}01} & {\rm M7.2\pm0.6} & 0.02\pm0.10 & 12.59\pm0.04 & -0.31\pm0.09^a \\ {\rm NTC~013\text{-}05} & {\rm M7.5\pm0.6} & 0.02\pm0.06 & 12.69\pm0.04 & -0.04\pm0.08 \\ {\rm NTC~013\text{-}05} & {\rm M7.5\pm0.6} & 0.05\pm0.07 & 12.48\pm0.04 & 0.01\pm0.08 \\ {\rm NTC~013\text{-}05} & {\rm M7.5\pm0.6} & 0.05\pm0.07 & 12.48\pm0.04 & 0.01\pm0.08 \\ {\rm NTC~013\text{-}06} & {\rm M7.7\pm0.7} & 0.26\pm0.07 & 12.22\pm0.06 & 0.00\pm0.19 \\ {\rm NTC~042\text{-}03} & {\rm M7.6\pm0.6} & 0.06\pm0.07 & 12.22\pm0.06 & 0.00\pm0.09 \\ {\rm NTC~043\text{-}06} & {\rm M8.2\pm0.6} & 0.06\pm0.07 & 11.80\pm0.04 & 0.31\pm0.08 \\ {\rm NTC~013\text{-}06} & {\rm M7.7\pm0.7} & 0.26\pm0.07 & 12.67\pm0.04 & 0.30\pm0.09 \\ {\rm NTC~013\text{-}06} & {\rm M8.2\pm0.7} & 0.01\pm0.07 & 12.58\pm0.14 & 0.16\pm0.16 \\ {\rm NTC~015\text{-}06} & {\rm M9.1\pm0.7} & 0.00\pm0.09 & 12.76\pm0.13 & 0.02\pm0.16 \\ {\rm NTC~012\text{-}02} & {\rm M9.4\pm0.9} & 0.31\pm0.01 & 1.408\pm0.09 & -0.03\pm0.14 \\ {\rm L99~312} & {\rm M6.0\pm0.2} & 0.13\pm0.04 & 12.26\pm0.08 & -0.14\pm0.09 \\ {\rm L99~332} & {\rm M6.0\pm0.2} & 0.19\pm0.04 & 12.27\pm0.05 & 0.39\pm0.07 \\ {\rm L99~367} & {\rm M6.5\pm0.5} & 0.05\pm0.04 & 12.86\pm0.12 & 0.16\pm0.14 \\ {\rm L99~382} & {\rm M6.0\pm0.2} & 0.19\pm0.04 & 12.27\pm0.05 & 0.39\pm0.07 \\ {\rm L99~363} & {\rm M8.0\pm0.2} & 0.00\pm0.04 & 13.05\pm0.05 & 0.06\pm0.07 \\ {\rm L99~363} & {\rm M8.0\pm0.2} & 0.00\pm0.04 & 13.05\pm0.05 & 0.06\pm0.07 \\ {\rm L99~363} & {\rm M8.0\pm0.2} & 0.00\pm0.04 & 13.05\pm0.05 & 0.06\pm0.07 \\ {\rm L99~363} & {\rm M8.0\pm0.2} & 0.00\pm0.04 & 13.05\pm0.05 & $	NTC 053-01	$M6.1 \pm 0.6$	0.18 ± 0.06	10.75 ± 0.04	0.45 ± 0.08					
$\begin{array}{c} {\rm NTC~014-05} & {\rm M6.3} \pm 0.6 & 0.04 \pm 0.07 & 12.96 \pm 0.05 & 0.26 \pm 0.09 \\ {\rm NTC~011-02} & {\rm M6.4} \pm 0.6 & 0.00 \pm 0.18 & 12.29 \pm 0.05 & -0.04 \pm 0.10 \\ {\rm NTC~055-06} & {\rm M6.4} \pm 0.7 & 0.06 \pm 0.06 & 12.45 \pm 0.07 & 0.24 \pm 0.10 \\ {\rm NTC~051-01} & {\rm M6.5} \pm 0.6 & 0.17 \pm 0.06 & 11.66 \pm 0.04 & 0.03 \pm 0.08 \\ {\rm NTC~062-01} & {\rm M6.8} \pm 0.7 & 0.19 \pm 0.08 & 13.15 \pm 0.08 & 0.13 \pm 0.11 \\ {\rm NTC~014-04} & {\rm M6.8} \pm 0.6 & 0.22 \pm 0.06 & 11.06 \pm 0.04 & 0.16 \pm 0.08 \\ {\rm NTC~022-05} & {\rm M6.8} \pm 0.6 & 0.22 \pm 0.06 & 11.06 \pm 0.04 & 0.14 \pm 0.08 \\ {\rm NTC~045-02} & {\rm M7.1} \pm 0.6 & 0.00 \pm 0.10 & 12.59 \pm 0.04 & -0.31 \pm 0.09^a \\ {\rm NTC~045-02} & {\rm M7.2} \pm 0.6 & 0.00 \pm 0.10 & 12.59 \pm 0.04 & -0.31 \pm 0.09^a \\ {\rm NTC~011-01} & {\rm M7.2} \pm 0.6 & 0.02 \pm 0.06 & 12.69 \pm 0.04 & -0.04 \pm 0.08 \\ {\rm NTC~013-05} & {\rm M7.5} \pm 0.6 & 0.05 \pm 0.07 & 12.48 \pm 0.04 & 0.01 \pm 0.08 \\ {\rm NTC~013-05} & {\rm M7.5} \pm 0.6 & 0.05 \pm 0.07 & 12.48 \pm 0.04 & 0.01 \pm 0.08 \\ {\rm NTC~013-06} & {\rm M7.7} \pm 0.7 & 0.26 \pm 0.07 & 12.67 \pm 0.06 & 0.00 \pm 0.09 \\ {\rm NTC~013-06} & {\rm M7.7} \pm 0.7 & 0.26 \pm 0.07 & 12.67 \pm 0.04 & 0.30 \pm 0.09 \\ {\rm NTC~013-06} & {\rm M8.2} \pm 0.6 & 0.06 \pm 0.07 & 11.80 \pm 0.04 & 0.31 \pm 0.08 \\ {\rm NTC~015-06} & {\rm M9.1} \pm 0.7 & 0.00 \pm 0.09 & 12.76 \pm 0.13 & 0.02 \pm 0.16 \\ {\rm NTC~012-02} & {\rm M9.4} \pm 0.9 & 0.31 \pm 0.11 & 14.08 \pm 0.09 & -0.03 \pm 0.14 \\ \hline \\ & & & & & & & & & & & & & & & & &$	NTC 044-04	$M6.2 \pm 0.6$	0.02 ± 0.06	11.82 ± 0.04	0.15 ± 0.08					
$\begin{array}{c ccccccccccccccccccccccccccccccccccc$	NTC 055-02	$M6.3 \pm 0.6$	0.24 ± 0.06	12.19 ± 0.04	0.29 ± 0.08					
$\begin{array}{c} {\rm NTC~075\text{-}06} & {\rm M6.4 \pm 0.7} & 0.06 \pm 0.06 & 12.45 \pm 0.07 & 0.24 \pm 0.10 \\ {\rm NTC~051\text{-}01} & {\rm M6.5 \pm 0.6} & 0.17 \pm 0.06 & 11.66 \pm 0.04 & 0.03 \pm 0.08 \\ {\rm NTC~062\text{-}01} & {\rm M6.8 \pm 0.7} & 0.19 \pm 0.08 & 13.15 \pm 0.08 & 0.13 \pm 0.11 \\ {\rm NTC~014\text{-}04} & {\rm M6.8 \pm 0.6} & 0.22 \pm 0.06 & 11.06 \pm 0.04 & 0.16 \pm 0.08 \\ {\rm NTC~022\text{-}05} & {\rm M6.8 \pm 0.6} & 0.53 \pm 0.07 & 12.42 \pm 0.04 & 0.24 \pm 0.08 \\ {\rm NTC~045\text{-}02} & {\rm M7.1 \pm 0.6} & 0.00 \pm 0.10 & 12.59 \pm 0.04 & -0.31 \pm 0.09^{\circ} \\ {\rm NTC~062\text{-}03} & {\rm M7.2 \pm 0.6} & 0.00 \pm 0.15 & 12.75 \pm 0.06 & 0.02 \pm 0.12 \\ {\rm NTC~011\text{-}01} & {\rm M7.2 \pm 0.6} & 0.02 \pm 0.06 & 12.69 \pm 0.04 & -0.04 \pm 0.08 \\ {\rm NTC~013\text{-}05} & {\rm M7.5 \pm 0.6} & 0.05 \pm 0.07 & 12.48 \pm 0.04 & 0.01 \pm 0.08 \\ {\rm NTC~013\text{-}05} & {\rm M7.5 \pm 0.6} & 0.05 \pm 0.07 & 12.48 \pm 0.04 & 0.01 \pm 0.08 \\ {\rm NTC~013\text{-}05} & {\rm M7.7 \pm 0.7} & 0.26 \pm 0.07 & 12.67 \pm 0.04 & 0.30 \pm 0.09 \\ {\rm NTC~013\text{-}06} & {\rm M7.7 \pm 0.7} & 0.26 \pm 0.07 & 12.67 \pm 0.04 & 0.30 \pm 0.09 \\ {\rm NTC~043\text{-}06} & {\rm M8.2 \pm 0.6} & 0.06 \pm 0.07 & 12.58 \pm 0.14 & 0.16 \pm 0.16 \\ {\rm NTC~015\text{-}01} & {\rm M8.2 \pm 0.7} & 0.01 \pm 0.07 & 12.58 \pm 0.14 & 0.16 \pm 0.16 \\ {\rm NTC~015\text{-}06} & {\rm M9.1 \pm 0.7} & 0.00 \pm 0.09 & 12.76 \pm 0.13 & 0.02 \pm 0.16 \\ {\rm NTC~012\text{-}02} & {\rm M9.4 \pm 0.9} & 0.31 \pm 0.11 & 14.08 \pm 0.09 & -0.03 \pm 0.14 \\ \hline & {\rm IC~348:~outer~sample} \\ \hline \\ & {\rm L99~205} & {\rm M6.0 \pm 0.2} & 0.13 \pm 0.04 & 11.43 \pm 0.04 & 0.38 \pm 0.06 \\ {\rm L99~312} & {\rm M6.0 \pm 0.2} & 0.19 \pm 0.04 & 12.27 \pm 0.05 & 0.39 \pm 0.07 \\ {\rm L99~367} & {\rm M6.5 \pm 0.5} & 0.30 \pm 0.04 & 12.86 \pm 0.12 & 0.16 \pm 0.14 \\ {\rm L99~382} & {\rm M6.5 \pm 0.5} & 0.30 \pm 0.04 & 12.86 \pm 0.12 & 0.16 \pm 0.14 \\ {\rm L99~382} & {\rm M6.5 \pm 0.5} & 0.30 \pm 0.04 & 13.05 \pm 0.05 & 0.06 \pm 0.07 \\ {\rm L99~407} & {\rm M7.0 \pm 0.5} & 0.40 \pm 0.20 & 13.77 \pm 0.04 & 0.11 \pm 0.17 \\ {\rm L99~363} & {\rm M8.0 \pm 0.2} & 0.00 \pm 0.04 & 13.05 \pm 0.05 & 0.06 \pm 0.07 \\ {\rm L99~405} & {\rm M8.0 \pm 0.2} & 0.09 \pm 0.06 & 9.79 \pm 0.04 & 0.10 \pm 0.07 \\ {\rm MHO~5} & {\rm M6.25 \pm 0.2} & 0.01 \pm 0.06 & 9.28 \pm 0.04 & 0.30 \pm 0.07 \\ {\rm CFHT-Tau~1} & {\rm M7~\pm 0.5} & 0.30 \pm 0.10 & 11.44 $	NTC 014-05		0.04 ± 0.07	12.96 ± 0.05	0.26 ± 0.09					
$\begin{array}{c} {\rm NTC~051\text{-}01} & {\rm M6.5\pm0.6} & 0.17\pm0.06 & 11.66\pm0.04 & 0.03\pm0.08 \\ {\rm NTC~062\text{-}01} & {\rm M6.8\pm0.7} & 0.19\pm0.08 & 13.15\pm0.08 & 0.13\pm0.11 \\ {\rm NTC~014\text{-}04} & {\rm M6.8\pm0.6} & 0.22\pm0.06 & 11.06\pm0.04 & 0.16\pm0.08 \\ {\rm NTC~022\text{-}05} & {\rm M6.8\pm0.6} & 0.53\pm0.07 & 12.42\pm0.04 & 0.24\pm0.08 \\ {\rm NTC~045\text{-}02} & {\rm M7.1\pm0.6} & 0.00\pm0.10 & 12.59\pm0.04 & -0.31\pm0.09^{\rm a} \\ {\rm NTC~062\text{-}03} & {\rm M7.2\pm0.6} & 0.00\pm0.10 & 12.59\pm0.06 & 0.02\pm0.12 \\ {\rm NTC~011\text{-}01} & {\rm M7.2\pm0.6} & 0.00\pm0.15 & 12.75\pm0.06 & 0.02\pm0.12 \\ {\rm NTC~013\text{-}05} & {\rm M7.5\pm0.6} & 0.05\pm0.07 & 12.48\pm0.04 & -0.04\pm0.08 \\ {\rm NTC~042\text{-}03} & {\rm M7.5\pm0.6} & 0.05\pm0.07 & 12.48\pm0.04 & 0.01\pm0.08 \\ {\rm NTC~013\text{-}05} & {\rm M7.5\pm0.6} & 0.05\pm0.07 & 12.48\pm0.04 & 0.01\pm0.08 \\ {\rm NTC~013\text{-}06} & {\rm M7.7\pm0.7} & 0.26\pm0.07 & 12.67\pm0.04 & 0.30\pm0.09 \\ {\rm NTC~013\text{-}06} & {\rm M7.7\pm0.7} & 0.26\pm0.07 & 12.67\pm0.04 & 0.30\pm0.09 \\ {\rm NTC~013\text{-}06} & {\rm M8.2\pm0.6} & 0.06\pm0.07 & 12.58\pm0.14 & 0.16\pm0.16 \\ {\rm NTC~015\text{-}06} & {\rm M8.2\pm0.7} & 0.01\pm0.07 & 12.58\pm0.14 & 0.16\pm0.16 \\ {\rm NTC~015\text{-}06} & {\rm M9.1\pm0.7} & 0.00\pm0.09 & 12.76\pm0.13 & 0.02\pm0.16 \\ {\rm NTC~012\text{-}02} & {\rm M9.4\pm0.9} & 0.31\pm0.11 & 14.08\pm0.09 & -0.03\pm0.14 \\ \hline & {\rm IC~348:~outer~sample} \\ \hline \\ {\rm L99~205} & {\rm M6.0\pm0.2} & 0.13\pm0.04 & 11.43\pm0.04 & 0.38\pm0.06 \\ {\rm L99~312} & {\rm M6.0\pm0.2} & 0.19\pm0.04 & 12.27\pm0.05 & 0.39\pm0.07 \\ {\rm L99~367} & {\rm M6.5\pm0.5} & 0.05\pm0.04 & 12.60\pm0.08 & -0.14\pm0.09 \\ {\rm L99~382} & {\rm M6.5\pm0.5} & 0.05\pm0.04 & 12.69\pm0.07 & 0.37\pm0.10 \\ {\rm L99~363} & {\rm M8.0\pm0.2} & 0.00\pm0.04 & 13.05\pm0.05 & 0.06\pm0.07 \\ {\rm L99~363} & {\rm M8.0\pm0.2} & 0.00\pm0.04 & 13.20\pm0.07 & 0.15\pm0.09 \\ \hline & {\rm V410~Anon~13} & {\rm M6\pm1.0} & 0.42\pm0.06 & 10.00\pm0.04 & 0.25\pm0.11 \\ {\rm V410~Anon~13} & {\rm M6\pm1.0} & 0.42\pm0.06 & 10.00\pm0.04 & 0.25\pm0.11 \\ {\rm V410~Anon~13} & {\rm M6\pm0.2} & 0.09\pm0.06 & 9.79\pm0.04 & 0.10\pm0.07 \\ {\rm MHO~5} & {\rm M6.25\pm0.2} & 0.01\pm0.06 & 9.28\pm0.04 & 0.30\pm0.07 \\ {\rm CFHT-Tau~1} & {\rm M7\pm0.5} & 0.30\pm0.10 & 11.14\pm0.08 & 0.02\pm0.11 \\ {\rm CFHT-Tau~2} & {\rm M8\pm0.5} & 0.00\pm0.10 & 11.41\pm0.06 & 0.16\pm0.10 \\ \hline \end{array}$	NTC 011-02	$M6.4 \pm 0.6$	0.00 ± 0.18	12.29 ± 0.05	-0.04 ± 0.13					
$\begin{array}{c} {\rm NTC~062\text{-}01} & {\rm M6.8\pm0.7} & 0.19\pm0.08 & 13.15\pm0.08 & 0.13\pm0.11 \\ {\rm NTC~014\text{-}04} & {\rm M6.8\pm0.6} & 0.22\pm0.06 & 11.06\pm0.04 & 0.16\pm0.08 \\ {\rm NTC~022\text{-}05} & {\rm M6.8\pm0.6} & 0.53\pm0.07 & 12.42\pm0.04 & 0.24\pm0.08 \\ {\rm NTC~045\text{-}02} & {\rm M7.1\pm0.6} & 0.00\pm0.10 & 12.59\pm0.04 & -0.31\pm0.09^{\rm a} \\ {\rm NTC~062\text{-}03} & {\rm M7.2\pm0.6} & 0.00\pm0.15 & 12.75\pm0.06 & 0.02\pm0.12 \\ {\rm NTC~011\text{-}01} & {\rm M7.2\pm0.6} & 0.02\pm0.06 & 12.69\pm0.04 & -0.04\pm0.08 \\ {\rm NTC~013\text{-}05} & {\rm M7.5\pm0.6} & 0.02\pm0.06 & 12.69\pm0.04 & -0.04\pm0.08 \\ {\rm NTC~013\text{-}05} & {\rm M7.5\pm0.6} & 0.05\pm0.07 & 12.48\pm0.04 & 0.01\pm0.08 \\ {\rm NTC~013\text{-}05} & {\rm M7.6\pm0.6} & 0.10\pm0.07 & 12.22\pm0.06 & 0.00\pm0.09 \\ {\rm NTC~013\text{-}06} & {\rm M7.7\pm0.7} & 0.26\pm0.07 & 12.67\pm0.04 & 0.30\pm0.09 \\ {\rm NTC~043\text{-}06} & {\rm M8.2\pm0.6} & 0.06\pm0.07 & 11.80\pm0.04 & 0.31\pm0.08 \\ {\rm NTC~105\text{-}01} & {\rm M8.2\pm0.7} & 0.01\pm0.07 & 12.58\pm0.14 & 0.16\pm0.16 \\ {\rm NTC~015\text{-}06} & {\rm M9.1\pm0.7} & 0.00\pm0.09 & 12.76\pm0.13 & 0.02\pm0.16 \\ {\rm NTC~012\text{-}02} & {\rm M9.4\pm0.9} & 0.31\pm0.11 & 14.08\pm0.09 & -0.03\pm0.14 \\ \hline & IC~348: \ {\rm outer~sample} $				12.45 ± 0.07	0.24 ± 0.10					
$\begin{array}{c ccccccccccccccccccccccccccccccccccc$					0.03 ± 0.08					
$\begin{array}{c} {\rm NTC~022-05} & {\rm M6.8\pm0.6} & 0.53\pm0.07 & 12.42\pm0.04 & 0.24\pm0.08 \\ {\rm NTC~045-02} & {\rm M7.1\pm0.6} & 0.00\pm0.10 & 12.59\pm0.04 & -0.31\pm0.09^{\rm a} \\ {\rm NTC~062-03} & {\rm M7.2\pm0.6} & 0.00\pm0.15 & 12.75\pm0.06 & 0.02\pm0.12 \\ {\rm NTC~011-01} & {\rm M7.2\pm0.6} & 0.02\pm0.06 & 12.69\pm0.04 & -0.04\pm0.08 \\ {\rm NTC~013-05} & {\rm M7.5\pm0.6} & 0.05\pm0.07 & 12.48\pm0.04 & 0.01\pm0.08 \\ {\rm NTC~042-03} & {\rm M7.6\pm0.6} & 0.10\pm0.07 & 12.22\pm0.06 & 0.00\pm0.09 \\ {\rm NTC~013-06} & {\rm M7.7\pm0.7} & 0.26\pm0.07 & 12.67\pm0.04 & 0.30\pm0.09 \\ {\rm NTC~013-06} & {\rm M7.7\pm0.7} & 0.26\pm0.07 & 12.67\pm0.04 & 0.30\pm0.09 \\ {\rm NTC~013-06} & {\rm M8.2\pm0.6} & 0.06\pm0.07 & 12.58\pm0.14 & 0.16\pm0.16 \\ {\rm NTC~015-01} & {\rm M8.2\pm0.7} & 0.01\pm0.07 & 12.58\pm0.14 & 0.16\pm0.16 \\ {\rm NTC~015-06} & {\rm M9.1\pm0.7} & 0.00\pm0.09 & 12.76\pm0.13 & 0.02\pm0.16 \\ {\rm NTC~012-02} & {\rm M9.4\pm0.9} & 0.31\pm0.11 & 14.08\pm0.09 & -0.03\pm0.14 \\ \hline \\ & & & & & & & & & & & & & & & & &$										
$\begin{array}{c} {\rm NTC~045-02} & {\rm M7.1\pm0.6} & 0.00\pm0.10 & 12.59\pm0.04 & -0.31\pm0.09^{\rm a} \\ {\rm NTC~062-03} & {\rm M7.2\pm0.6} & 0.00\pm0.15 & 12.75\pm0.06 & 0.02\pm0.12 \\ {\rm NTC~011-01} & {\rm M7.2\pm0.6} & 0.02\pm0.06 & 12.69\pm0.04 & -0.04\pm0.08 \\ {\rm NTC~013-05} & {\rm M7.5\pm0.6} & 0.05\pm0.07 & 12.48\pm0.04 & 0.01\pm0.08 \\ {\rm NTC~042-03} & {\rm M7.6\pm0.6} & 0.10\pm0.07 & 12.22\pm0.06 & 0.00\pm0.09 \\ {\rm NTC~013-06} & {\rm M7.7\pm0.7} & 0.26\pm0.07 & 12.67\pm0.04 & 0.30\pm0.09 \\ {\rm NTC~013-06} & {\rm M7.7\pm0.7} & 0.26\pm0.07 & 12.67\pm0.04 & 0.30\pm0.09 \\ {\rm NTC~013-06} & {\rm M8.2\pm0.6} & 0.06\pm0.07 & 11.80\pm0.04 & 0.31\pm0.08 \\ {\rm NTC~105-01} & {\rm M8.2\pm0.7} & 0.01\pm0.07 & 12.58\pm0.14 & 0.16\pm0.16 \\ {\rm NTC~015-06} & {\rm M9.1\pm0.7} & 0.00\pm0.09 & 12.76\pm0.13 & 0.02\pm0.16 \\ {\rm NTC~012-02} & {\rm M9.4\pm0.9} & 0.31\pm0.11 & 14.08\pm0.09 & -0.03\pm0.14 \\ \hline \\ & & & & & & & & & & & & & & & & &$										
$\begin{array}{c} {\rm NTC~062\text{-}03} & {\rm M7.2\pm0.6} & 0.00\pm0.15 & 12.75\pm0.06 & 0.02\pm0.12 \\ {\rm NTC~011\text{-}01} & {\rm M7.2\pm0.6} & 0.02\pm0.06 & 12.69\pm0.04 & -0.04\pm0.08 \\ {\rm NTC~013\text{-}05} & {\rm M7.5\pm0.6} & 0.05\pm0.07 & 12.48\pm0.04 & 0.01\pm0.08 \\ {\rm NTC~042\text{-}03} & {\rm M7.6\pm0.6} & 0.10\pm0.07 & 12.22\pm0.06 & 0.00\pm0.09 \\ {\rm NTC~013\text{-}06} & {\rm M7.7\pm0.7} & 0.26\pm0.07 & 12.67\pm0.04 & 0.30\pm0.09 \\ {\rm NTC~043\text{-}06} & {\rm M8.2\pm0.6} & 0.66\pm0.07 & 12.67\pm0.04 & 0.30\pm0.09 \\ {\rm NTC~043\text{-}06} & {\rm M8.2\pm0.6} & 0.66\pm0.07 & 11.80\pm0.04 & 0.31\pm0.08 \\ {\rm NTC~105\text{-}01} & {\rm M8.2\pm0.7} & 0.01\pm0.07 & 12.58\pm0.14 & 0.16\pm0.16 \\ {\rm NTC~015\text{-}06} & {\rm M9.1\pm0.7} & 0.00\pm0.09 & 12.76\pm0.13 & 0.02\pm0.16 \\ {\rm NTC~012\text{-}02} & {\rm M9.4\pm0.9} & 0.31\pm0.11 & 14.08\pm0.09 & -0.03\pm0.14 \\ \hline \\ & & & & & & & & & & & & & & & & &$										
$\begin{array}{c} {\rm NTC~011\text{-}01} & {\rm M7.2\pm0.6} & 0.02\pm0.06 & 12.69\pm0.04 & -0.04\pm0.08 \\ {\rm NTC~013\text{-}05} & {\rm M7.5\pm0.6} & 0.05\pm0.07 & 12.48\pm0.04 & 0.01\pm0.08 \\ {\rm NTC~042\text{-}03} & {\rm M7.6\pm0.6} & 0.10\pm0.07 & 12.22\pm0.06 & 0.00\pm0.09 \\ {\rm NTC~013\text{-}06} & {\rm M7.7\pm0.7} & 0.26\pm0.07 & 12.67\pm0.04 & 0.30\pm0.09 \\ {\rm NTC~043\text{-}06} & {\rm M8.2\pm0.6} & 0.06\pm0.07 & 11.80\pm0.04 & 0.31\pm0.08 \\ {\rm NTC~105\text{-}01} & {\rm M8.2\pm0.7} & 0.01\pm0.07 & 12.58\pm0.14 & 0.16\pm0.16 \\ {\rm NTC~015\text{-}06} & {\rm M9.1\pm0.7} & 0.00\pm0.09 & 12.76\pm0.13 & 0.02\pm0.16 \\ {\rm NTC~015\text{-}06} & {\rm M9.1\pm0.7} & 0.00\pm0.09 & 12.76\pm0.13 & 0.02\pm0.16 \\ {\rm NTC~012\text{-}02} & {\rm M9.4\pm0.9} & 0.31\pm0.11 & 14.08\pm0.09 & -0.03\pm0.14 \\ \hline \\ \hline & & & & & & & & & & & & & & & &$										
$\begin{array}{c ccccccccccccccccccccccccccccccccccc$										
$\begin{array}{cccccccccccccccccccccccccccccccccccc$										
$\begin{array}{c ccccccccccccccccccccccccccccccccccc$										
$\begin{array}{c ccccccccccccccccccccccccccccccccccc$										
$\begin{array}{c ccccccccccccccccccccccccccccccccccc$										
$\begin{array}{c ccccccccccccccccccccccccccccccccccc$										
$ \begin{array}{c ccccccccccccccccccccccccccccccccccc$										
$ \begin{array}{c ccccccccccccccccccccccccccccccccccc$										
$\begin{array}{c ccccccccccccccccccccccccccccccccccc$	N1C 012-02	10.4 ± 0.9	0.31 ± 0.11	14.08 ± 0.09	-0.03 ± 0.14					
$\begin{array}{c ccccccccccccccccccccccccccccccccccc$			C 348: outer sa	mple						
$\begin{array}{c ccccccccccccccccccccccccccccccccccc$										
$\begin{array}{c ccccccccccccccccccccccccccccccccccc$										
$\begin{array}{c ccccccccccccccccccccccccccccccccccc$										
$\begin{array}{c ccccccccccccccccccccccccccccccccccc$										
$\begin{array}{c ccccccccccccccccccccccccccccccccccc$										
$ \begin{array}{c ccccccccccccccccccccccccccccccccccc$										
$\begin{array}{c ccccccccccccccccccccccccccccccccccc$										
$\begin{array}{c ccccccccccccccccccccccccccccccccccc$	L99 405	$M8.0 \pm 0.2$	0.00 ± 0.04	13.20 ± 0.07	0.15 ± 0.09					
$\begin{array}{cccccccccccccccccccccccccccccccccccc$	Taurus									
$\begin{array}{cccccccccccccccccccccccccccccccccccc$	V410 Anon 13	$M6 \pm 1.0$	0.42 ± 0.06	10.00 ± 0.04	0.25 ± 0.11					
$ \begin{array}{cccccccccccccccccccccccccccccccccccc$										
$ \begin{array}{llllllllllllllllllllllllllllllllllll$	•									
CFHT-Tau 2 $M8 \pm 0.5$ 0.00 ± 0.10 11.41 ± 0.06 0.16 ± 0.10		$M7 \pm 0.5$		11.14 ± 0.08						
	CFHT-Tau 4	$M7 \pm 0.5$		9.15 ± 0.03						
CFHT-Tau 3 $M9 \pm 0.5$ 0.00 ± 0.10 11.63 ± 0.03 0.00 ± 0.09	CFHT-Tau 2	$M8 \pm 0.5$	0.00 ± 0.10	11.41 ± 0.06	0.16 ± 0.10					
	CFHT-Tau 3	$M9 \pm 0.5$	0.00 ± 0.10	11.63 ± 0.03	0.00 ± 0.09					

^aThis object has $K_S - L' = 0.23 \pm 0.04$, much bluer than the other objects in the sample. Based on its JHK_SL' colors, it appears to be a background late-type giant star. It is excluded from the analysis.

Spectral	IC 348	IC 348	Total
Type	core	core + outer	(IC 348 + Taurus)
5.7 - 6.4 6.5 - 7.4 7.5 - 8.4 8.5 - 9.4 all types	8/10 5/6 4/5 1/2 18/23 (73% ± 19%)	$ \begin{array}{c} 10/13 \\ 8/9 \\ 6/7 \\ 1/2 \\ 25/31 \\ (75\% \pm 17\%) \end{array} $	$ \begin{array}{c} 13/16 \\ 10/11 \\ 7/8 \\ 1/3 \\ 31/38 \\ (77\% \pm 15\%) \end{array} $

Note. — The percentages of sources with IR excesses and their errors were evaluated using a Monte Carlo technique which accounts for both measurement errors and Poisson counting statistics. See Appendix A.

 ${\it TABLE~3}$ Flat Blackbody Reprocessing Disk: Maximum Excess (in mags)

Spectral Type	ΔJ	ΔH	ΔK_S	$\Delta L'$	$\Delta M'$
M0 M1 M2 M3 M4 M5 M6	0.27 0.23 0.20 0.18 0.16 0.14 0.12	0.38 0.35 0.33 0.31 0.28 0.26 0.24	0.63 0.60 0.56 0.52 0.49 0.45 0.42	1.38 1.32 1.26 1.20 1.13 1.05 0.98	1.78 1.72 1.66 1.59 1.52 1.44 1.36
M7 M8 M9	$0.10 \\ 0.09 \\ 0.08$	0.22 0.19 0.17	$0.38 \\ 0.34 \\ 0.31$	$0.89 \\ 0.81 \\ 0.73$	1.27 1.17 1.08

Note. — Transmission profiles for the $J\!H\!K_S$ bands are from 2MASS, while those for the L' and M' bands are from the MKO system.